

POLITECNICO DI TORINO

Department of Mechanical and Aerospace Engineering
Master degree course in Aerospace Engineering

Master Degree Thesis

Extraction of relevant data from experimental test and matching with FEA



Supervisors:

Prof. Christian Maria Firrone

Ing. Antonio Giuseppe D'Ettore

Candidate:

Matteo Nicita

Student Number: 271806

Academic Year 2021-2022

Abstract

In the last decades a great effort has been done in designing more and more efficient engines with higher performances in order to cut environmental impact of aeronautical industry. In this perspective, it is crucial to reduce both weight and consumptions by using the most advanced technologies and materials. Yet, this exposes to unavoidable risks such as aeromechanical phenomena and instabilities.

Arias project's main goal is precisely to deep understand such occurrences with the scope to provide a guideline for future applications and design. This is possible as a result of the cooperation of the major European constructors and universities. This work of thesis, thanks to the opportunity given by Avio Aero, is framed in such context. In particular, this thesis deals with the study of experimental data, which have been collected for ARIAS, in order to find the best way to extract damping factor and other relevant data among several methods proposed. All the aforementioned methods have formerly been tested on elementary functions and then applied to actual data distribution. Furthermore, a comparison between results obtained both from experimental data and FEA was made.

AKNOWLEDGEMENTS

Vorrei ringraziare innanzitutto il Prof. Christian Maria Firrone per aver reso possibile questo progetto di tesi in collaborazione con Avio Aero e per avermi seguito in questo percorso.

Un grande grazie va anche agli Ing. Antonio Giuseppe D'Ettole e Martin Tomek non solo per l'enorme aiuto datomi in questi mesi di lavoro sempre con pazienza e disponibilità, ma anche per avermi dato la possibilità di conoscere le dinamiche aziendali e avermi fatto crescere molto sotto il profilo professionale.

Alla mia famiglia, a mia nonna e a Sabina per avermi insegnato l'importanza di impegnarsi e lavorare sodo per raggiungere i propri obiettivi e per avermi lasciato sempre libero nelle mie scelte supportandole tutte.

A Michele e Piero, compagni di università e di vita. Grazie per aver condiviso le ansie e le gioie di questo percorso per cinque lunghi anni tra i banchi del Poli, e grazie per aver sempre creduto in me più di quanto io non credessi in me stesso.

Ai Codeghiani, che in un periodo difficile come quello della pandemia, siete riusciti a diventare la mia famiglia a Torino, rendendo questi anni insieme i più spensierati della mia vita. Questo traguardo è la prova definitiva che non vi ammorberò più con le parole “tesi” e “azienda”.

TABLE OF CONTENTS

Acknowledgements.....	III
List of figures.....	VI
List of tables	VIII
1. Introduction	1
1.1 The aircraft engine	3
1.1.1 Turbojet.....	4
1.1.2 Turbofan.....	5
1.1.3 Turboprop.....	6
1.1.4 Turboshaft	6
1.2 Low Pressure Turbines (LPT).....	6
2. Bladed disk Dynamics.....	8
2.1 Cyclic Symmetry.....	8
2.2 Finite Element discretization.....	9
2.3 Real and complex modes	11
2.4 Modal Analysis	14
2.5 Nodal diameters and FreND diagram.....	16
3. Aeroelasticity.....	18
3.1 Aerodynamic of turbines.....	19
3.1.1 Potential disturbs	19
3.1.2 Flutter	20
4. Linear Forced Response	25
4.1 Loads classification.....	25
4.1.1 Static loads	25
4.1.2 Dynamic loads.....	26
5. ARiAS Introduction.....	28
5.1 Spinning Test on Stargate Rig.....	29
5.1.1 Blade Tip Timing system	31
5.2 Test Article Design	32
6. Data fitting Methods.....	35
6.1 Data format	35
6.2 Methods used	36

6.2.1	Gauss-2 parameters	37
6.2.2	Gauss-1parameter.....	37
6.2.3	Kumaraswamy Distribution	38
6.2.4	Single Degree of Freedom Method	38
6.3	Methods comparison	39
7.	Matching with fea.....	44
7.1	Modal analysis	44
7.2	Tuned Configuration	45
7.3	Mistuned Mass 01 Configuration.....	46
7.4	Mistuning Mass 0001	48
7.5	Tuned + Damper Steel	49
7.6	Tuned + Damper Aluminum	52
8.	Conclusions	55
Bibliography.....		56

LIST OF FIGURES

Figure 1.1 Joule-Bryton Cycle	3
Figure 1.2 Aircraft Engine	4
Figure 1.3 Turbojet	5
Figure 1.4 Turbofan	5
Figure 1.5 Turboprop	6
Figure 1.6 Turboshaft.....	6
Figure 1.7 Low pressure turbine	7
Figure 2.1 Example of structures in cyclic symmetry.....	9
Figure 2.2 Cyclic sector extraction	9
Figure 2.3 Representation of a stationary wave at two frozen instants.....	13
Figure 2.4 Representation of a rotating travelling wave at two frozen instants	13
Figure 2.5 DOF partition for the nth sector.....	14
Figure 2.6 Example of typical modeshapes.....	16
Figure 2.7 FreND diagram	17
Figure 2.8 Example of veering.....	17
Figure 3.1 Collar's triangle.....	18
Figure 3.2 Example of a 2DOF system.....	21
Figure 3.3 Unstable, Oscillatory and Stable system response	22
Figure 3.4 Aerodynamic coupling on a blade row	23
Figure 3.5 Example of an aeroplot	24
Figure 3.6 Aerodynamic coupling as a function of IBPA	24
Figure 4.1 Example of zig-zag diagram.....	27
Figure 4.2 Example of Campbell diagram	27
Figure 5.1Test rig.....	29
Figure 5.2 Test rig scheme	30
Figure 5.3 ToA variations	31
Figure 5.4 Mistuning Mass	32
Figure 5.5 Underplatform damper.....	32
Figure 6.1 Frequency vs. Amplitude and Time vs. Amplitude plots o a generic test.....	35
Figure 6.2 Data distribution after filtering	36
Figure 6.3 Gaussian curve	37
Figure 6.4 Mass-Spring-Damper system	38
Figure 6.5 Parameters for Q-factor calculation	39
Figure 6.6 Triangular function.....	40
Figure 6.7 Sinusoidal function.....	40
Figure 6.8 Parabolic function	41
Figure 6.9 Methods applied to analytical functions.....	42
Figure 6.10 Shot 203 M1, Accel - Blade 75	43
Figure 7.1 Tuned Configuration – Modeshapes for Mode 1 and 2	45
Figure 7.2 Tuned Configuration – Modeshapes for Mode 1 and 2	45
Figure 7.3 Mistuned Mass 01 - Modeshape for Mode 1 blades 0 and 1	47
Figure 7.4 Mistuned Mass 01 - Modeshape for Mode 2 blades 0 and 1	47
Figure 7.5 Mistuned Mass 01 - Adjacent blades FRFs.....	48
Figure 7.6 Mistuned Mass 0001 - Modeshape for Mode 1 blades 0 and 1	49
Figure 7.7 Mistuned Mass 0001 - Modeshape for Mode 2 blades 0 and 1	49

Figure 7.8 Tuned + Damper Steel Configuration – Modeshapes for Mode 1 and 2	50
Figure 7.9 Tuned + Damper Steel Configuration – Modeshapes for Mode 1 and 2	50
Figure 7.10 Tuned + Damper Steel - Adjacent blades FRFs	51
Figure 7.11 Tuned + Damper Alu Configuration – Modeshapes for Mode 1 and 2.....	52
Figure 7.12 Tuned + Damper Alu Configuration – Modeshapes for Mode 1 and 2.....	52
Figure 7.13 Frequency per blade	53
Figure 7.14 TA and Dampers closeup.....	53
Figure 7.15 Underplatform Damper effect on average Peak Amplitude.....	53

LIST OF TABLES

Table 1 Methods Comparison	43
Table 2 Q-factor and Quadratic Residue using different methods	43
Table 3 Tuned Configuration results	45
Table 4 Mistuned Mass 01 results	46
Table 5 Mistuned Mass 0001 results	48
Table 6 Tuned + Damper Steel results	50
Table 7 Tuned + Damper Alu results	52

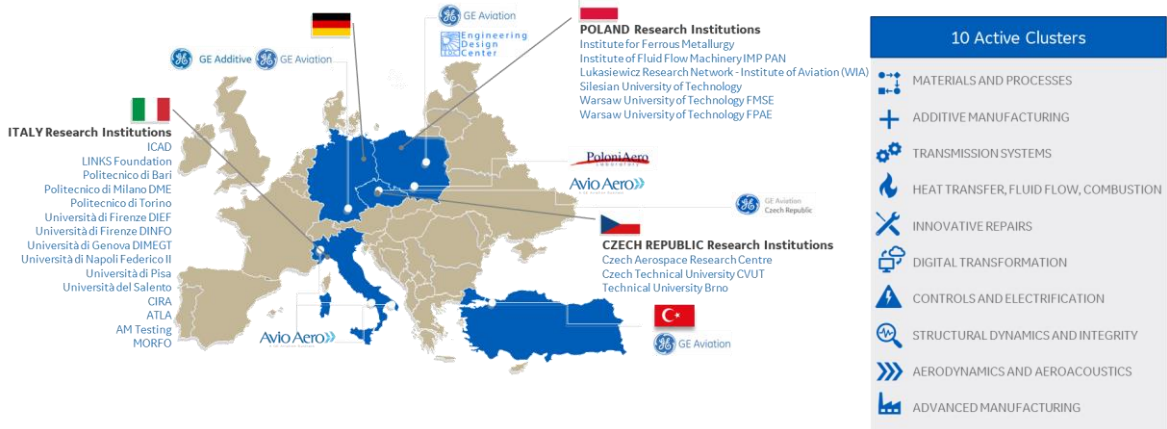
1. INTRODUCTION

This thesis work has been developed in the *E-TDCs (European Technology Development Clusters)*, a platform built by AvioAero and other European GE partner, in conjunction with many European universities, including *Politecnico di Torino* (PoliTo).



E-TDC in a Nutshell

This work has been done in the *Structural Dynamic and Integrity Cluster* focused on research activities relates to the Aeromechanics: studies related to HCF (High Cycle Fatigue) problems due to greater vibrational phenomena, and to Flutter Analysis. This discipline has become of great interest from the designers, as it ensures that these high performance engines operate safely.



32 parties: 21 Research Institutions, 3 SMEs and 8 GE Affiliates

As this subject is of great complexity, to match industries needs FSI (Fluid-Structure Interaction) is still treated in simplified forms, from decoupled and linearized methods. If when validating a design more accurate and time consuming solutions can be adopted, in the first designing phase is of fundamental importance to have available fast and effective tools to give immediate feedback on aeromechanical behavior and design choices impact.

1.1 The aircraft engine

Throughout aviation history propulsion system design issue lead to different solutions. Due to the huge complexity of this field, only the most important architecture will be shown in this chapter.

The main principle that governs all of the aircraft engines is the Newton's Third Law: “*for every force acting on a body, there is an opposite and equal reaction*”.

In practice, this principle is exploited by taking air from the atmosphere and energizing the incoming flow and then expelling it at higher speed. Energization of the flow can be obtained by compressing and then providing heat to it. The difference in momentum of the air flow is nothing more than the total impulse given to the engine in the opposite direction. Since the engine is assembled to an aircraft body, the resulting force is transmitted to the entire aircraft. This force is commonly called *Thrust* and is proportional to the variation of velocity and to the mass flow rate of air managed. Yet, a great change in flow speed results in lower propulsive efficiency; for this reason, in modern aviation, the focus is to obtain the same difference in momentum by minimizing velocity exit speed and maximizing air mass flow rate.

From a thermodynamic point of view, aircraft engines most commonly use Joule-Brayton cycle, which is shown in the picture below:

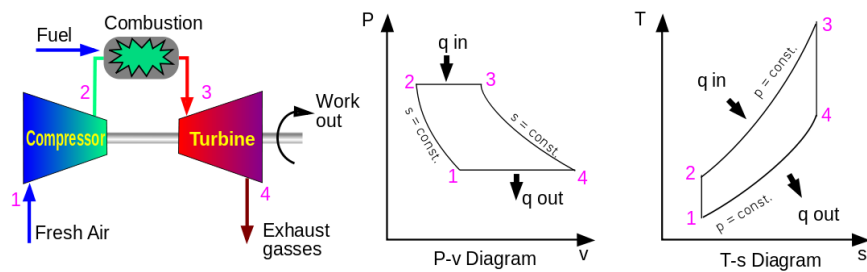


Figure 1.1 Joule-Bryton Cycle

As we can see from the previous scheme, the architecture in this case of study (multi-shaft engine) consists of:

- **Air intake:** It is basically a duct that lets air enter to the engine regulating pressure and mass flow downstream;
- **Compressor:** It is typically divided into a former compressor, which deals with lower pressure and a second compressor. These two parts are usually called Low and High Pressure Turbines (LPT, HPT). The main purpose of this organ is to increase air pressure;

- **Combustion chamber:** Here fuel is injected and mixed with the air; the mix is then burnt in order to increase gases temperature. Combustion often occurs far from stoichiometric ratio, using a mix rich in air;
- **Turbine:** As the compressor, it is often divided in Low Pressure Turbine (LPT) and High Pressure Turbine (HPT) and it expands the exhaust gas. It is used to gain the necessary power to make the Compressor work.
- **Nozzle:** It allows the exhaust gases to gain momentum by accelerating and thus obtaining thrust.

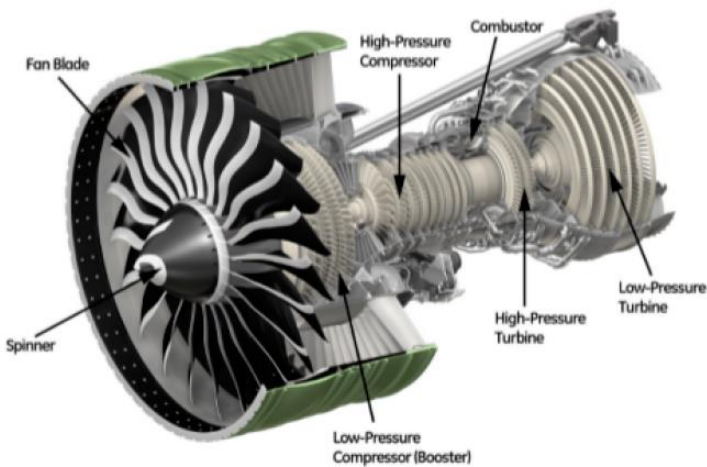


Figure 1.2 Aircraft Engine

1.1.1 Turbojet

This is one of the former architectures and somehow the starting point for next propulsion systems. It has a simpler structure since there are only one Compressor and Turbine. This type of engine mostly rely on generating thrust by accelerating air flow, rather than intaking more air compromising efficiency; for this reason, it has been replaced by more efficient architecture in almost every civil application.

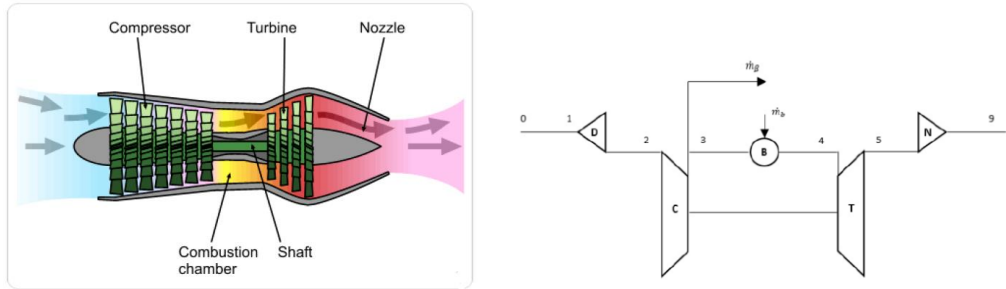


Figure 1.3 Turbojet

1.1.2 Turbofan

This architecture can be considered as an evolution of turbojet concept. Indeed, it operates on turbojet efficiency limits by dividing the air entering the engine into two different flows. The major part of the flow then follows a different path, which consists only of a few compressor/turbine stages and fuel combustion is not involved (cold flow). The other fraction of air flow follows the traditional turbojet path (hot flow). By adopting this architecture we are allowed to obtain the same thrust by accelerating less the overall flow and intaking more air. An important parameter for this kind of engines is the *by-pass ratio*, which is the ratio between the cold and the hot flow.

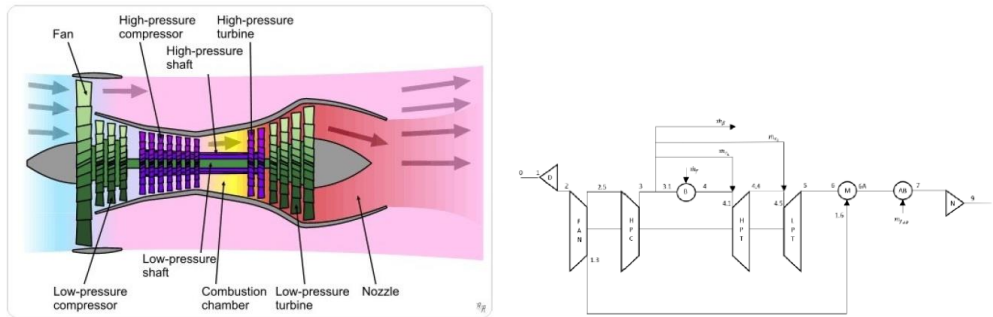


Figure 1.4 Turbofan

1.1.3 Turboprop

The concept behind this architecture is to exaggerate turbofan architecture. In this case, there is not a fan inserted in a duct; yet, an external propeller is installed. By doing so, all the thrust is developed by the propeller, which accelerates a little a much greater air mass flow. Even though this concept seems to provide the greatest efficiency among all the architectures shown, it has strict limits on aircraft speed. Indeed, since the propeller may have large diameter, the tangential speed on the blade tip, combined with the external air flow, may cause unpredictable supersonic effects.

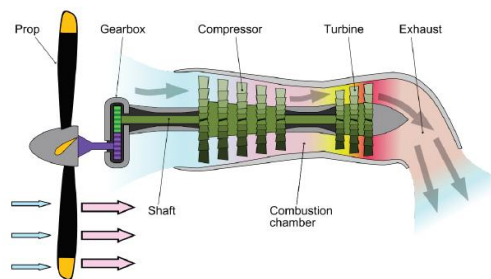


Figure 1.5 Turboprop

1.1.4 Turboshaft

The main objective of this configuration is not to directly produce thrust. Indeed, in this kind of engine the turbine does not develop the exact same power needed by the compressor. Turboshaft engines are usually adopted to gain extra power on the shaft to be transmitted to other mechanical organs, such as helicopter fan.

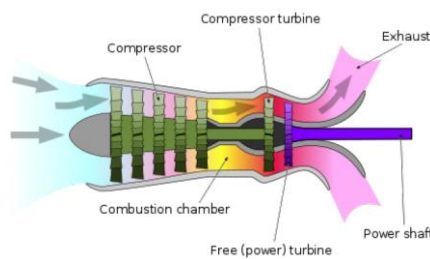


Figure 1.6 Turboshaft

1.2 Low Pressure Turbines (LPT)

Since Avio Aero puts a lot of effort in LPT design and manufacture, this section will be a closeup on how LPT works in detail. As said before, the main objective of a turbine is to extract mechanical work from an expanding gas in order to provide enough power to make the compressor work.

A macroscopic differentiation can be done based on how the gas flow exits the turbine related to its rotational axis:

- *Axial*: outgoing flow is parallel to the rotational axis;
- *Radial*: outgoing flow is orthogonal to the rotational axis (radial).

Another classification can be done whether the pressure drop throughout the turbine occurs in the first stage (*Impulse Turbine*) or in multiple stages (*Reaction Turbine*).

A stage is the elementary unit of a turbine. A turbine can be made of one or more stages and every stage consists of:

- **Stator**: it is fixedly linked to the engine structure, and it is used to set the right flow direction in order for it to enter properly the rotoric interblade channel;
- **Rotor**: it is the rotating part that actually extract work from the flow and transfer it to the shaft.

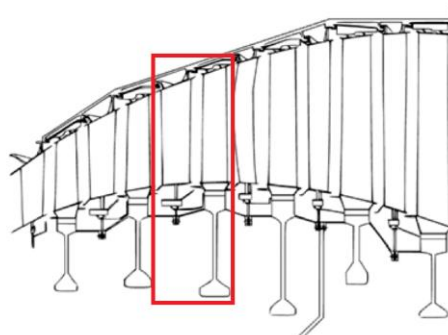


Figure 1.7 Low pressure turbine

2. BLADED DISK DYNAMICS

Since turbine organs are usually under nonstationary and vibrational forcing, it is interesting to look at how excitation affects blades and disk behavior. Indeed, some of the phenomena that may occur, such as instability or resonance, are related to structural properties and may lead to disastrous consequences. In order to avoid damages and improve reliability and safety of the structure, further studies on vibrational nodes are required.

2.1 Cyclic Symmetry

By the term *bladed disk*, we usually refer to turbomachine rotors. It consists of a series of blades that interact with the flow and a disk, which is divided into as many segments as many blades there are. According to similarities between blades and disk segments that allow us to identify a pattern in the sequence of blades, we can group one ore more blades with their related disk segments into sectors. In case we are able to obtain the original disk by a revolution of a single sector around rotational axis, we are talking about *Cyclic Symmetry*, which is basically a tool that help us get information about the whole disk by studying one of its sectors. It is important to notice how the disk part cannot be neglected in the study since it may affect dynamic behavior of the sector and change mode shapes and natural frequencies.

A single sector is characterized by an angle $\alpha = \frac{2\pi}{N}$, where N is the number of sectors. If all the blades are the same, a sector consists of only one blade and N is the number of blades.

A complete study in cyclic symmetry also requires information about boundary conditions such as rotational speed and temperature.



Figure 2.1 Example of structures in cyclic symmetry

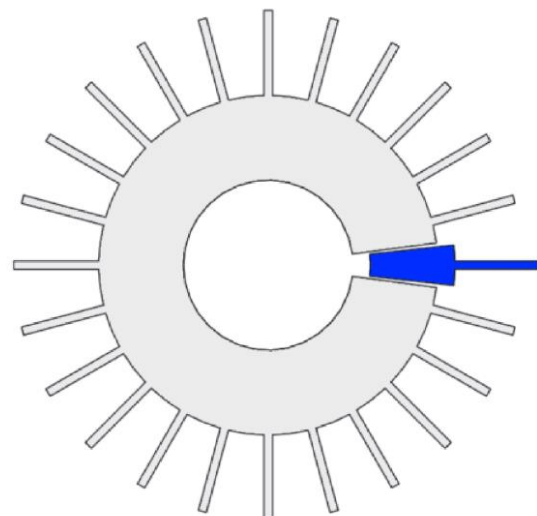


Figure 2.2 Cyclic sector extraction

2.2 Finite Element discretization

Referring to a generic body, it is possible to discretize it in Finite Elements and define the *Equation of Motion*:

$$[M] \cdot \{\ddot{x}\} + [K] \cdot \{x\} = \{F\} \quad \dots \dots \dots \quad (2.1)$$

Where:

- x : is the position vector relative to the degrees of freedom of the nodes ;
- M : is the mass matrix;
- K : is the stiffness matrix;
- F : is the external forces vector.

Let us suppose that a number n of nodes is being considered for the entire structure, then x and F vectors have $3n \times 1$ dimension, while M and K matrices have $3n \times 3n$ dimensions.

When working with Cyclic Symmetry it is convenient to use cylindrical coordinate $\{\rho, \theta, z\}$, with z parallel to rotational axis. In this case:

$$x = \rho \cos(\theta) \quad (2.2)$$

$$y = \rho \sin(\theta) \quad (2.2)$$

It is possible to rearrange the elements of the x vector so that we can group them in subset, each one representative for a sector. Hence, there will be N subset.

In this way the terms in Eq 2.1 can be rewritten as:

$$\{x\} = \begin{Bmatrix} x_1 \\ x_2 \\ x_3 \\ \vdots \\ x_{N-1} \\ x_N \end{Bmatrix} \quad \{F\} = \begin{Bmatrix} F_1 \\ F_2 \\ F_3 \\ \vdots \\ F_{N-1} \\ F_N \end{Bmatrix} \quad (2.3)$$

$$[M] = \begin{bmatrix} M_0 & M_1 & M_2 & \cdots & M_2 & M_1 \\ M_1 & M_0 & M_1 & \cdots & M_3 & M_2 \\ M_2 & M_1 & M_0 & \cdots & M_4 & M_3 \\ \vdots & \vdots & \vdots & \ddots & \vdots & \vdots \\ M_2 & M_3 & M_4 & \cdots & M_0 & M_1 \\ M_1 & M_2 & M_3 & \cdots & M_1 & M_0 \end{bmatrix} \quad (2.3a)$$

$$[K] = \begin{bmatrix} K_0 & K_1 & K_2 & \cdots & K_2 & K_1 \\ K_1 & K_0 & K_1 & \cdots & K_3 & K_2 \\ K_2 & K_1 & K_0 & \cdots & K_4 & K_3 \\ \vdots & \vdots & \vdots & \ddots & \vdots & \vdots \\ K_2 & K_3 & K_4 & \cdots & K_0 & K_1 \\ K_1 & K_2 & K_3 & \cdots & K_1 & K_0 \end{bmatrix} \quad (2.3b)$$

[M] and [K] matrices obtain will also be divided into sub-matrices $[M_n]$ and $[K_n]$ (for $h = 0, \dots, N/2$ if N is even or $h = 0, \dots, (N-1)/2$ if N is odd). Each nth-matrice is symmetrical as well as [M] and [K] and, defining n_s the number of DOF in a single sector, it has $n_s \times n_s$ dimensions. A further sorting is $[M_n]$ elements can be done by differentiating:

- Left-hand side nodes defined as those nodes at left interface between 2 consecutive sectors;
- Right-hand side nodes defined as those nodes at right interface between 2 consecutive sectors;
- Inner nodes.

2.3 Real and complex modes

By resolving the eigenproblem below, it is possible to evaluate both modeshapes $\{u_i\}$ (eigenvectors) and natural frequencies ω_i (eigenvalues):

$$([K] - \omega_i^2 \cdot [M]) \cdot \{u_i\} = \{0\} \quad (2.4)$$

According to the elements value of eigenvectors we can have different modeshapes, which can be grouped in three categories:

- **Stationary modes:** it is characterized by a single real eigenvalue and a single eigenvector.
In this case Φ_n can only assume the values below:
 $\Phi_n = 0$: all the blades vibrate in-phase and the number of nodal diameters is 0

$$\{u_{ni}\} = \{u_{(n+1)i}\} \quad \forall n \quad (2.5)$$

$\Phi_n = \pm\pi$: the modeshape is still the same, yet the blades vibrate in anti-phase. This is only possible with an even number of blades. In this case the maximum number of nodal diameters is $N/2$.

$$\{u_{ni}\} = -\{u_{(n+1)i}\} \quad \forall n \quad (2.6)$$

- **Rotating modes:** while former cases existed for 0 or $\pm\pi$ values of Φ_n , rotating modes describe all the intermediate cases, meaning that for any other value of Φ_n :

$$\{u_{ni}\} \neq \{u_{(n+1)i}\} \quad \forall n \quad (2.7)$$

The modeshapes are also defined by the same eigenvalue.

Thanks to cyclic symmetry, rotating $\{u_i\}$ by an angle of α_n allows to get next sector modeshape $\{u'_i\}$. Yet, it is convenient to define for a given eigenvalue, which is common to all the sectors, a couple of orthogonal complex eigenvectors $\{u_i\}$ and $\{\bar{u}_l\}$. By doing so that we can express every sector's modeshape as a linear combination of these two vectors:

$$\{u'_i\} = c\{u_i\} + s\{\bar{u}_l\} \quad (2.8)$$

Where, assuming a correct normalization of eigenvectors, it is possible to demonstrate that c and s coefficient can be written as:

$$c = \cos(\Phi_n) \quad (2.9)$$

$$s = -\sin(\Phi_n) \quad (2.10)$$

Similarly, by rotating of a sector angle $\{\bar{u}_l\}$ vector, we have $\{\bar{u}'_i\}$ which is orthogonal to $\{u'_i\}$ and can be written as:

$$\{\bar{u}'_i\} = -s\{u_i\} + c\{\bar{u}_l\} \quad (2.11)$$

Therefore:

$$\begin{Bmatrix} u'_i \\ \bar{u}'_l \end{Bmatrix} = \begin{bmatrix} cI_{Nns} & sI_{Nns} \\ -sI_{Nns} & cI_{Nns} \end{bmatrix} \cdot \begin{Bmatrix} u_i \\ \bar{u}_l \end{Bmatrix} = R \begin{Bmatrix} u_i \\ \bar{u}_l \end{Bmatrix} \quad (2.12)$$

What has been said on modes so far can be graphically noticed by adopting Eulerian formulation of complex numbers. Indeed, stationary and rotating modes' evolution in time can be rewritten as:

- Stationary (real eigenvalues):

$$Re(\{u_i\}e^{j\omega t}) = \{u_i\} \cos(\omega t) \quad (2.13)$$

- Rotating modes (complex eigenvalues), rearranging eigenvectors as $z_i = u_i + j\bar{u}_i$ and $\bar{z}_i = u_i - j\bar{u}_i$:

$$Re(\{z_i\}e^{j\omega t}) = \{u_i\} \cos(\omega t) - \{\bar{u}_i\} \sin(\omega t) \quad (2.14)$$

Moreover, while z_i rotates clockwise, \bar{z}_i rotates counterclockwise, meaning that the eventual relation between two adjacent sectors can be expressed as:

$$\{z_{(n-1)i}\} = \{z_{ni}\} e^{j\Phi_n} \quad (2.15)$$

And the time evolution of a sector's amplitude is the same as the previous sector shifted by a Φ_n/ω phase angle. That is also why Φ_n is also called Inter Blade Phase Angle (IBPA). Indeed, it represents the angular delay between adjacent sectors.

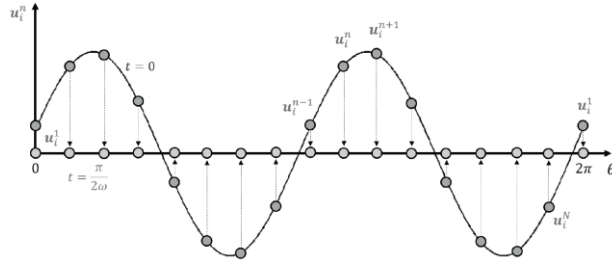


Figure 2.3 Representation of a stationary wave at two frozen instants

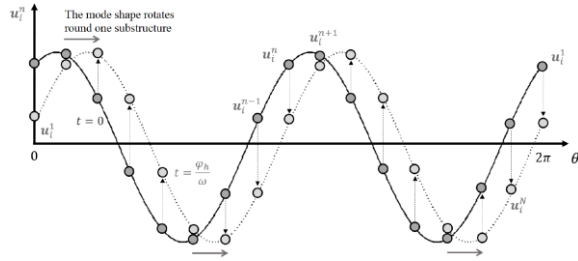


Figure 2.4 Representation of a rotating travelling wave at two frozen instants

Generally speaking, for a bladed disk we are more interested in complex modes rather than the real modes since the latter can then be interpreted as the sum of the two counter rotating traveling waves. Note that, if we want to investigate the mode shapes belonging to a the whole bladed disk, in addition to the rising of computational costs and processing time, we could only find real modes since FEM solvers resolve the eigenproblem 2.13 in the real domain.

2.4 Modal Analysis

Now that cyclic symmetry has been investigated, it is important to introduce different ways to perform modal analysis on a single sector in order to reduce computational cost and processing time. We have to keep in mind that FEM solvers usually find solution to modal eigenproblem only in the real domain, meaning that it may be convenient to find the two real orthogonal modes in which a rotating complex mode can be decomposed into.

The first method analyzed is the one proposed by D.J. Mead. Assuming that all the DOFs of a sector can be arranged in a vector like:

$$\{\mathbf{x}_s\} = \begin{pmatrix} \mathbf{x}_l \\ \mathbf{x}_i \\ \mathbf{x}_r \end{pmatrix} \quad (2.16)$$

Where $\{\mathbf{x}_l\}$ and $\{\mathbf{x}_r\}$ correspond to the DOFs which are respectively common to the considered sector and the sector on the left and right, while $\{\mathbf{x}_i\}$ groups all the internal DOFs that are not shared between two sectors.

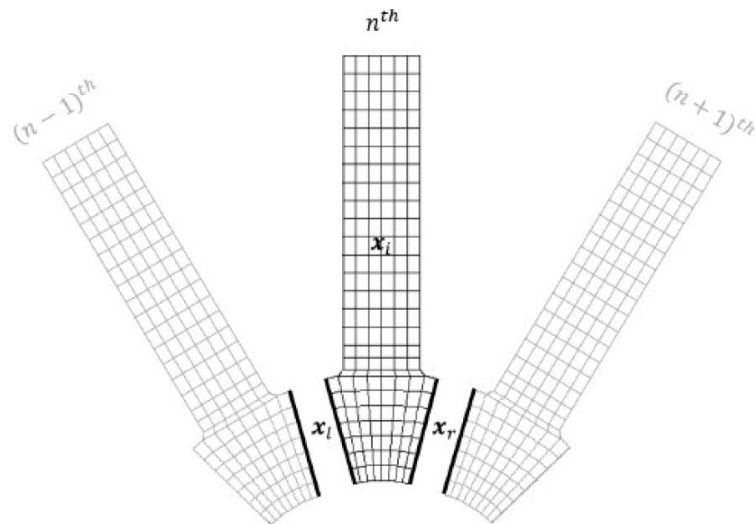


Figure 2.5 DOF partition for the n^{th} sector

For what have been said so far, in order for cyclic symmetry to be valid, DOFs on the left can be seen as DOFs on the right for the adjacent sector. This implies that $\{x_l\}$ and $\{x_r\}$ must be the same length. In particular, the $\{x_l\}$ must be obtained by rotating $\{x_r\}$ of exactly one IBPA.

$$\{x_s\} = \begin{Bmatrix} x_l \\ x_i \\ x_r \end{Bmatrix} = \begin{bmatrix} I & 0 \\ 0 & I \\ I e^{i\Phi_h} & 0 \end{bmatrix} \begin{Bmatrix} x_l^h \\ x_i^h \\ x_r^h \end{Bmatrix} = [T^h] \begin{Bmatrix} x_l^h \\ x_i^h \\ x_r^h \end{Bmatrix} = \{x_s^h\} \quad (2.17)$$

where $[T^h]$ is the Mead's transformation matrix and $\{x_s^h\}$ the DOF vector reduced in cyclic symmetry.

Similarly, also the forcing vector can be written as:

$$\{f_s\} = \begin{Bmatrix} f_l \\ f_i \\ f_r \end{Bmatrix} \quad (2.18)$$

Yet, due to equilibrium at interfaces:

$$\{f_r\}_n = \{f_l\}_{m+1} \quad (2.19)$$

And for cyclic symmetry:

$$\{f_r\} = \{f_l\} e^{j\Phi_n} \quad (2.20)$$

The mass and stiffness matrices of the single sector can also be decomposed in the same manner:

$$[M_s] = \begin{bmatrix} M_{ll} & M_{li} & M_{lr} \\ M_{il} & M_{ii} & M_{ir} \\ M_{rl} & M_{ir} & M_{rr} \end{bmatrix} \quad [K_s] = \begin{bmatrix} K_{ll} & K_{li} & K_{lr} \\ K_{il} & K_{ii} & K_{ir} \\ K_{rl} & K_{ir} & K_{rr} \end{bmatrix} \quad (2.21)$$

Defining:

$$\{z_i^n\} = \{\{x_l^n\}^T \quad \{x_i^n\}^T\}^T \quad (2.22)$$

The eigenproblem can be reformulated as:

$$([K^n] - w_i^2 [M^n]) \{z_i^n\} = 0 \quad (2.23)$$

And:

$$[K^n] = [T^n]^H [K^n] [T^n] \quad (2.24)$$

$$[M^n] = [T^n]^H [M^n] [T^n] \quad (2.25)$$

Where H refers to the Hermitian of $[T^n]$ matrix.

2.5 Nodal diameters and FreND diagram

The overall dynamic behavior of a bladed disk can be summed up by the FreND diagram, which shows the natural frequencies a function of number of nodal diameters for a chosen modeshape. It can be obtained by performing a lot of modal analysis, changing for every iteration the width of the sector angle; the wider the angle, the fewer nodal diameters. The total number of natural frequencies corresponds to the number of DOFs of the sector, meaning that a continuous body has an infinite number of DOFs. In our case, the number of DOFs is equal to the number of nodes chosen to discretize the structure.

Usually, the modeshapes of most interest are:

- **Edgewise mode (EW):** where the blade bends axially and the tip has the highest displacement;
- **Flapwise mode (FW):** where the blades bends tangentially and the tip has the highest displacement;
- **Flexural mode:** the highest displacement occurs tangentially at the mid-span;
- **Torsional mode:** there is a radial torsion along the blade axis.

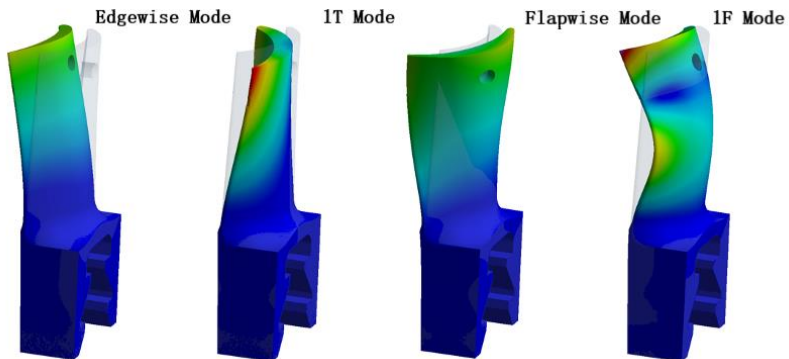


Figure 2.6 Example of typical modeshapes

An example of FreND diagram is shown below. As we can see, all the points corresponding to the same modeshape are grouped in families. Moreover, as the number of ND increases, the natural frequency for each family tends asymptotically to a certain value. In other words, for higher ND, natural frequency does not change much. This is because the higher the ND, the stiffer the disk gets, until it can be considered as motionless. At this point, on the right part of the diagram, it is like studying the blade alone, with weak coupling.

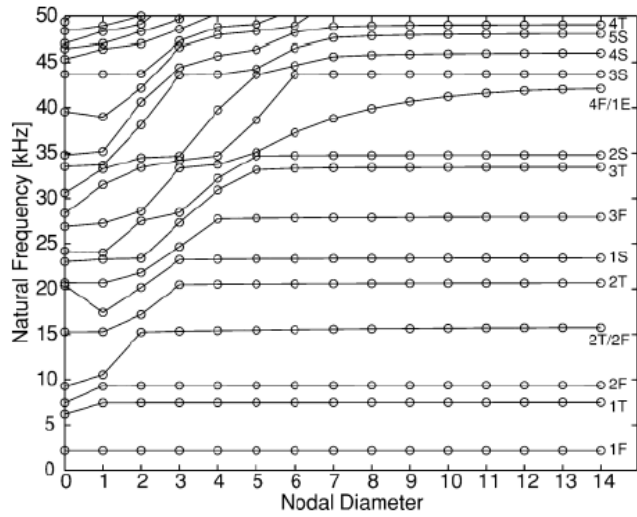


Figure 2.7 FreND diagram

By studying a bladed disk sector instead of a constrained blade it is possible to appreciate the effect of the disk taking part to the vibration by following the mode's frequency variation with ND: as ND increases the disk becomes more and more rigid until the frequency stabilizes to a constant value (Fig **Error! Reference source not found.**). While at lower ND the blade only frequency is comparable to the blade one and so the two are coupled together, at higher ND the disk's frequency grows exponentially so that it behaves essentially as rigid body.

It may happen that two different families of modeshapes have two really close natural frequencies. This phenomenon is called *veering*.

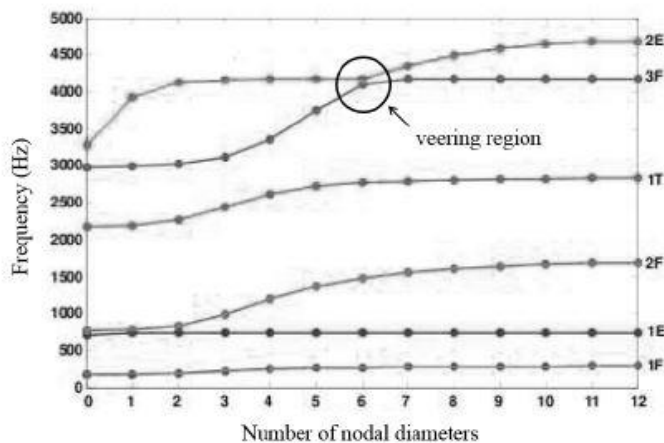


Figure 2.8 Example of veering

3. AEROELASTICITY

Since the forcing on the structure may come also from airflow; it is important to study how aerodynamic forces affect structural integrity and performances. Indeed, different kinds of aeromechanical instabilities may happen, which can lead to structure rupture long before than the classical fatigue analysis prediction. *Flutter* is an example, since aerodynamic forces enhance initial displacement. In particular, its origin may be related to the detachment of

the fluid flow from the airfoil (case of Stall Flutter), or to the detachment of the wake vortex from the LE (Transonic buffering) which both cause auto-excited vibrations. In

In order to better understand these kinds of phenomena, a new discipline is introduced: *Aeroelasticity*, which basically puts together:

- Structure dynamics: discipline where inertial and elastic forces are considered (Vibration mechanic)
- Flight Mechanic: with inertial and aerodynamic forces (Aerodynamic stability)
- Static aeroelasticity: when elastic and aerodynamic forces are present (Divergence)

As it is shown in the Collar's triangle below.

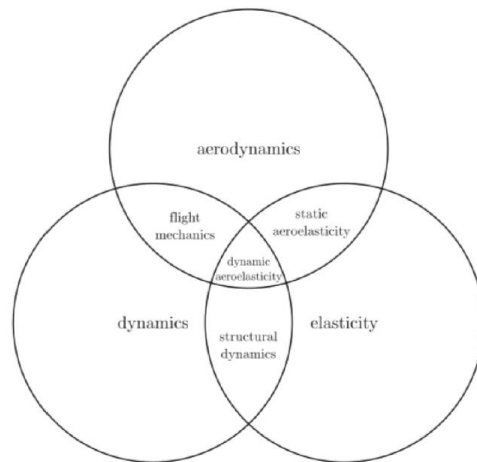


Figure 3.1 Collar's triangle

In general, the aerodynamic field represents the excitation source while elastic and inertial fields represent the system response. A deep understanding of how aerodynamic forcing interacts with the modal behavior of the structure allows to reduce engine weight and emissions and improve

performances. Indeed, by preventing aeroelastic phenomena thinner blades with higher aspect ratio and higher aerodynamic loads can be used.

3.1 Aerodynamic of turbines

The aerodynamic of turbines, despite the more traditional 1D formulation of an airfoil hit by air, can't be described without neglecting multi-dimensional aspects. This because the motion field is affected by interactions between rotating and non-rotating parts (stator and rotor), centrifugal forces and not negligible wall effects.

Aerodynamic inside turbomachinery is highly affected by a phenomenon called *stall condition*. It occurs when there is a strong pressure gradient between upstream and downstream, meaning that the flow cannot follow its regular path along the airfoil and air is forced to flow thorough near region. This leads to an acceleration of the flow near midspan.

The main consequence is that secondary flows that flow between stator and rotor blades are originated. The interaction between secondary flows and region with different pressure creates vortices.

Vortices can also originate when the wall flow encounter the fluid at the stagnation condition. In this case it can be observed a couple of vortices that shows a different behavior depending if those are in the suction side (vortices remain attached to the airfoil due to blade motion) or in the pressure side (those continue to proceed axially but moving towards the adjacent blade interacting also with the main fluid stream).

In conclusion, flow inside turbomachinery is far from being steady.

3.1.1 Potential disturbs

The velocity field flowing around an airfoil profile can be described by the gradient of a potential function under the hypothesis of $\nabla \times u = 0$. Moreover, the Kutta-Joukowsky theorem explains that, if the circulation around an airfoil profile, defined by the equation (3.1), is different from 0, then there will be a change of the velocity field also at the upstream and downstream. The so generated unsteady pressure leads to the creation of disturbs in terms of pressure waves which propagates at the

upstream and downstream and are characterized by an exponential decay governed by the Mach number, the pitch and axial distance.

$$\Gamma = \oint_{airfoil} \bar{u} \cdot \hat{n} \, dl \quad (3.1)$$

Shock waves

It consists of a sudden, unsteady recompression of the flow, which passes from a supersonic to a subsonic regime. This means that in a very narrow zone in close proximity of the shock wave, thermodynamic properties such as temperature, pressure and density have a literal discontinuity in the direction orthogonal to the wave. There are two kinds of shock waves: normal and oblique. The former is usually originated by choking condition while the latter is generally related to a deflection of supersonic flow. In this last case, velocity component parallel to the wave remains the same, meaning that it is possible for downstream flow to be still supersonic.

Wake

By the term Wake we refer to a region of turbulent flow due to the presence of a solid body. When pressure gradient and viscosity of the fluid are not negligible, it may happen that the flow hardly wets the entire surface of the body laminarly; yet the flow downstream of the body becomes turbulent. The wake area affects the surrounding flow field, modifying its velocity components and so aerodynamic efficiencies. Moreover, during the fluid motion, the wakes are modified by the pressure fields characterizing a circumferential a-periodicity when the fluid returns to the original reference system.

3.1.2 Flutter

Flutter is a very important phenomenon when talking about aeroelasticity. Indeed, it is due to asynchronous vibration caused by aerodynamic forces interacting with the structure. This results in an unstable condition of the structure, which ends up being self-excited. Under an energetic point of view it is possible to define the work per cycle of an exciting force as:

$$W_{cycle} = \int_t^{t+T} \int_S -p\hat{n} \cdot \vec{v} \, dS \, dt \quad (3.2)$$

The sign of W_{cycle} defines whether the system is stable or not. Indeed, when $W_{cycle} > 0$, then the work is done by the fluid on the blade and the system is stable and vice versa.

Classic flutter

Assuming a MDOF system like the one in the figure below, under the hypothesis of small oscillation ($\sin\theta = \theta$), it is possible to express aerodynamic force as a function of $h, \theta, I_h, I_\theta, m_h, m_\theta$:

$$\{F_a(t)\} = M_a\{\ddot{x}\} + C_a\{\dot{x}\} + K_a\{x\} \quad (3.3)$$

Where M, C and K refer to inertia, damping and stiffness matrix of the system and $\{x\}$ contains h and θ coordinates.

The overall governing equation, which considers all the forces acting on the system, either aerodynamic or not is:

$$M\{\ddot{x}\} + C\{\dot{x}\} + K\{x\} = \{F_a(t)\} + \{F_m(t)\} \quad (3.4)$$

Assuming that forces different from the aerodynamic ones can be neglected ($\{F_m(t)\} = 0$), then the equation becomes:

$$(M - M_a)\{\ddot{x}\} + (C - C_a)\{\dot{x}\} + (K - K_a)\{x\} = 0 \quad (3.5)$$

As flutter takes place when the real part of the system's eigenvalue becomes null, the blade's motion can be assumed purely harmonic.

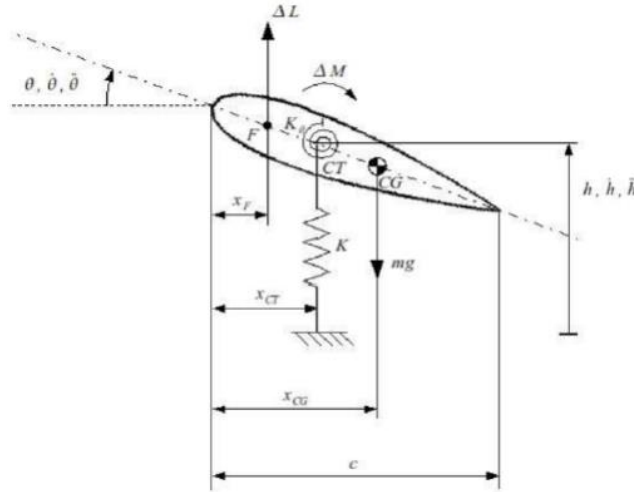


Figure 3.2 Example of a 2DOF system

General solution for the equation above is:

$$\{x(t)\} = \{\bar{x}_j\} e^{s_j t} \quad (3.6)$$

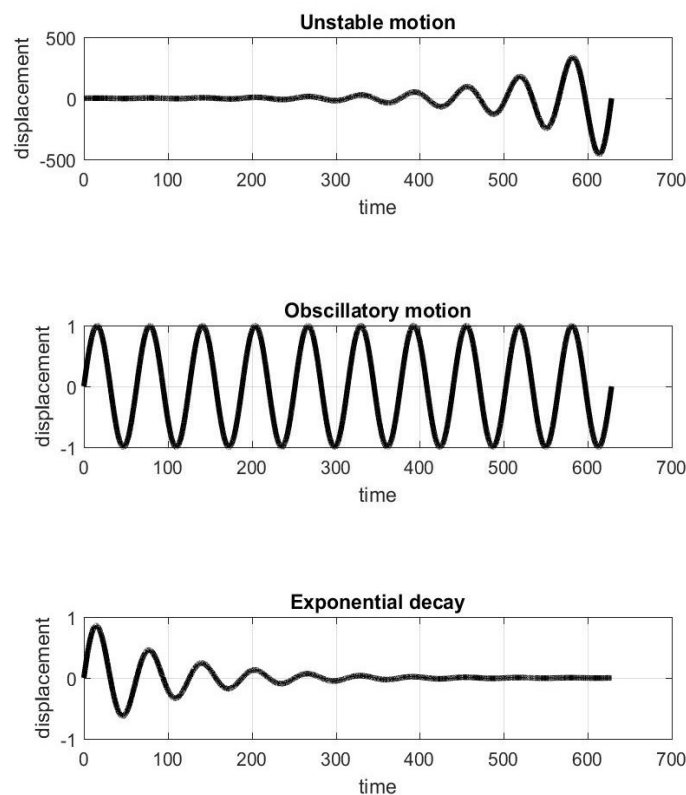
Where s_j is the complex eigenvalue: $s_j = \zeta_j + i\omega_j$

The real part of s_j defines the stability of the system:

- $Re(s_j) > 0$: the system is unstable

- $\text{Re}(s_j) = 0$: the system is oscillatory
- $\text{Re}(s_j) < 0$: the system is stable

Moreover, since flutter occurs for $\zeta_j > 0$, and being ζ a function of speed: $\zeta = f(v)$, then a critical velocity $v_{critical}$ can be determined. This means that velocity defines the stability of the system.



Flutter in turbomachines

Figure 3.3 Unstable, Oscillatory and Stable system response

What have been said about flutter on an isolated airfoil so far, can be extended to a blades row inside turbomachines. Yet, in this case it is important to take into account also coupling between adjacent blades, since vibrations of a blade can affect the dynamic behavior of the next one not only mechanically but also modifying flow field. Furthermore, also interaction between stator and rotor in the stage has to be considered.

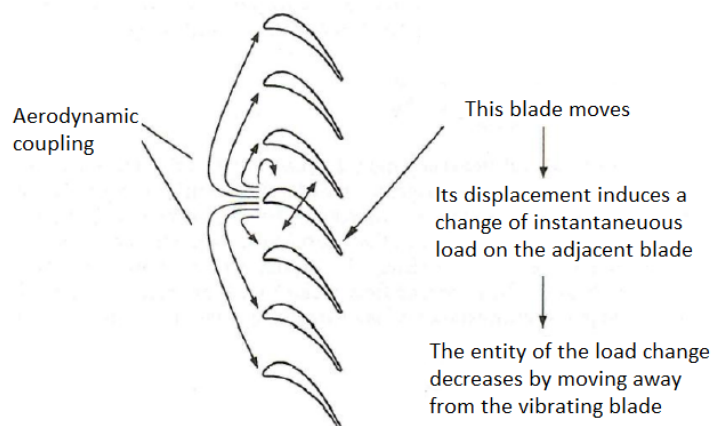


Figure 3.4 Aerodynamic coupling on a blade row

Things that mostly affect flutter are:

- IBPA: phase angle between adjacent blades
- Shroud: friction due to contact provides a further contribution to damping
- Shock waves: affect flow field by changing pressure loads
- Inlet and outlet condition: thermodynamic conditions of the flow affect aerodynamic damping
- Reduced frequency: which is defined as the ratio between a semi-chord of the airfoil profile and the period of the vibration cycle. This parameter defines on which regime the turbomachine is working; indeed, a low value of reduced frequency allow us to assume the flow quasi-static, otherwise it is unsteady.
- Mistuning: it is based on a intentional or unintentional non-homogeneity among all the blades. Mistuning mostly affect inertia, stiffness and damping matrixes.

In particular, it is possible to visualize how IBPA affect damping, and thus flutter. As it is shown in the figure below, the higher the IBPA the lower the interaction between blades. As a matter of fact, high values of IBPA means further blades, which are less likely to mutually interact. Moreover, by

expressing the influence as a function of IBPA, then we can see how it follows a sinusoidal trend. It is also clear how ζ is constant function of IBPA for blades ± 0 , since it is like studying an isolated profile, so influence is not noticeable.

Remembering the assumption of small displacement, it is possible to consider the problem linear, meaning that we are allowed to use superimposition principle to obtain *aeroplot*.

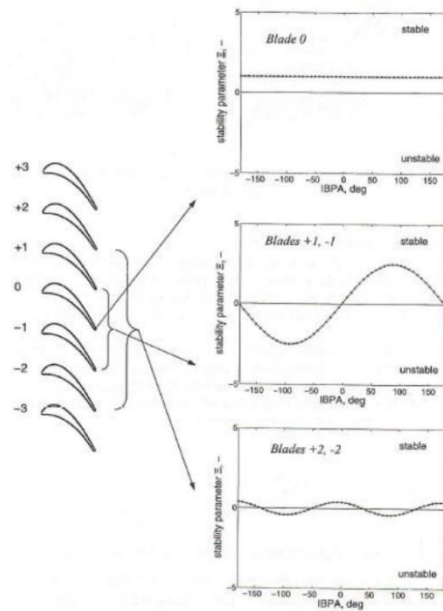


Figure 3.6 Aerodynamic coupling as a function of IBPA

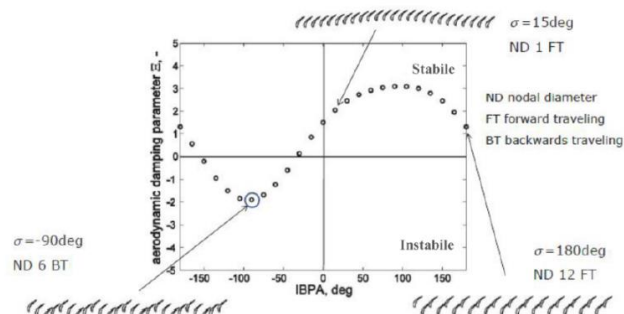


Figure 3.5 Example of an aeroplot

4.LINEAR FORCED RESPONSE

4.1 Loads classification

A general classification of loads that inside a Low Pressure Turbine (LPT) can be made by how forcing is dependent to time:

- *Static loads*: are mostly constant in time or have little variation;
- *Dynamic loads*: forces are a function of time;
- *Quasi-static loads*: are time dependent but are "slow" enough such that inertial effects can be ignored.

Yet, time dependency is related to the modal behavior of the system itself. As a matter of fact, the rate of change in the forcing should be compared to the natural frequencies of the system. When the frequency of the excitation is much lower than the natural one, then the load can be considered as static; otherwise, when the two frequencies have similar magnitude, the load must be considered ad dynamic.

4.1.1 Static loads

The main static loads in LPTs are:

- Steady pressure field: due to the necessary pressure gap between pressure and suction side on the blades. Defining the pressure filed – p – and the blade surface – S :

$$F_p = \int_S p \hat{n} dS \quad (4.1)$$

- Inertial load: due to the system being rotating, centrifugal forces must be taken into account:

$$F_c = \int_m dF_c = \int_V \rho \omega^2 r \hat{\mu}_r dV \quad (4.2)$$

- Temperature load: hot gases not only exchange with the blade mechanical work and energy, but also heat up the blades. This leads to the blades to undergo through additional load related to creep.
- Pre-Twist Load: twist is a sort of pre-loading of blades in order to achieve the right position of the airfoil respect the gas flux.

4.1.2 Dynamic loads

They are usually related to unsteady phenomena before and after rotor stage. The harmonic terms of the forcing is strongly related to the angular speed of the rotor and the number of blades in the row. This relation is expressed by a term called *Engine Order* (EO), which is defined as the ratio of the force frequency and the angular rotor speed:

$$EO = \frac{\omega}{\Omega} \quad (4.3)$$

In this case the excitation is *synchronous*, meaning that ω is an integer multiple of Ω . We usually divide high EO and low EO excitations since they are attributable to different phenomena. Indeed, high EOs are usually obtained by the interaction between stator and rotor rows. This is due to the fact that rotor blade face alternatively stator blade and interblade duct, so every blade undergoes an excitation as many times as how many blades there are in the row per rotation. On the other hand, low EOs are mostly linked to discontinuities like unbalanced rotating masses or asymmetry in tree's supports, interaction with distorted flow arriving from combustor.

Thanks to the periodicity given by spool rotation, the generic excitation can be expressed using Fourier series:

$$F(\alpha) = F_0 + \sum_{eo} F_c^{(eo)} \cos(eo \cdot \alpha) + F_s^{(eo)} \sin(eo \cdot \alpha) \quad (4.4)$$

Where $\alpha = \omega t$ and eo: engine order

This means that every term of the series gives a contribution in inducing synchronous vibrations in most of dynamic loads (excluding mechanical impacts and self-induced vibrations).

It is also important to highlight how rotational speed plays a massive role in determining natural frequencies of a system. Indeed, rotation induce a preload of the structure and makes it stiffer. How external loads and the system modal properties interact is described by the *Campbell's diagram*. This diagram has rotational speed on the x-axis and frequency on the y-axis and presents two different families of curves:

- Natural frequencies of the system. Theoretically these curves should be constant horizontal lines; yet, for what has been said about dependency by rotational speed, the curves tend to be upward slope;
- A pencil of straight lines starting from the origin and representing excitation. The higher the EO, the higher the slope.

Among all the points on the diagram, the ones candidates to be the condition for a possible resonance are the crossings between the two families of curves. Yet this represent only a sufficient but not necessary condition. Indeed, proper resonance occurs when the following relation is valid:

$$EO = m \cdot N \pm ND \quad (4.5)$$

Which is illustrated in the *zig-zag diagram*.

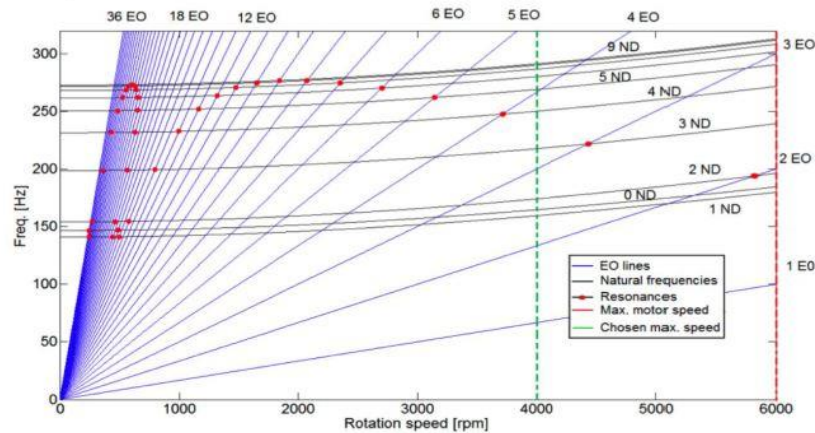


Figure 4.2 Example of Campbell diagram

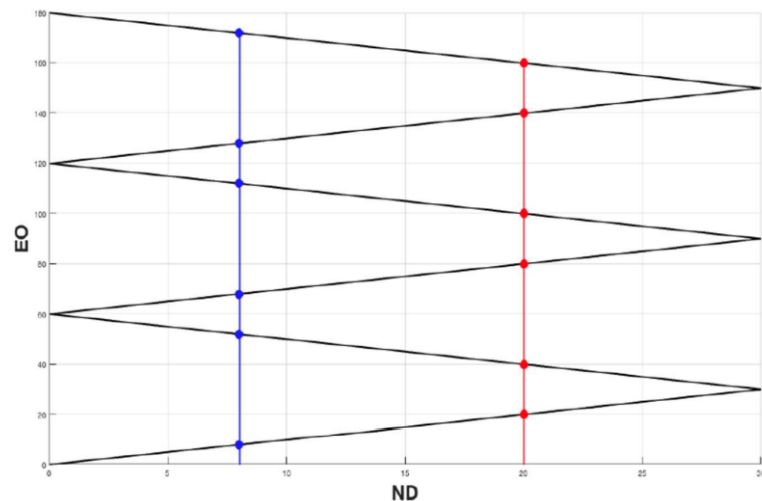


Figure 4.1 Example of zig-zag diagram

5. ARIAS INTRODUCTION

This work of thesis is framed inside the ARiAS Project, that stands for Advanced Research into Aeromechanical Solutions. The ARiAS research aims at improving competitiveness of the European aeronautic sector regarding the development of more cost-effective, safe, efficient and robust designs of aero engines. A deep understanding of *flutter* and *Forced Response (FR)* is necessary when trying to cut costs of product life cycle by reducing engine weight or using more advanced geometries. Since aeromechanical phenomena are still very difficult to study and predict, this research wants to provide new and more effective design methodologies.



Components that are most likely to undergo through failure due to aerodynamically induced vibrations are:

- Fan (Flutter and/or FR)
- High Pressure turbine (FR)
- Transonic compressors (flutter and/or FR)
- Low Pressure turbine (flutter and/or FR)
- High Pressure compressor (flutter and/or FR)
- Labyrinth seals (flutter)

To secure the ability in both establishing the influence of various structural and fluid characteristics on both propensity to flutter and forced response of blades and consequently using the enhanced understanding to aid the development of a range of preliminary design guidelines, ARiAS, together with the major European manufacturers, targets the following goals:

- Establishing a confidence level for the prediction of aerodynamic excitation/damping;
- Developing innovative monitoring techniques to prevent premature failures;
- Introducing active and passive dampers to reduce aeromechanical vibrations;
- Validating new configurations that include the use of intentional mistuning.

5.1 Spinning Test on Stargate Rig

The main focus of this work of thesis is to study experimental data acquired during the test campaign on Stargate rig. All the measurements have been performed on the rig in the picture below.

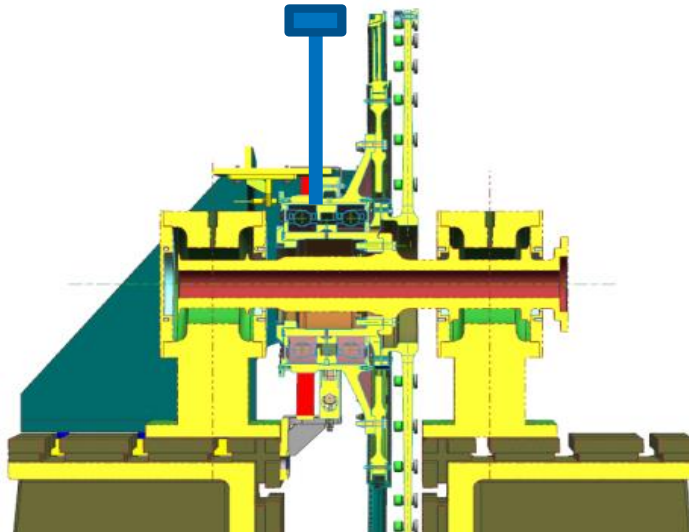


Figure 5.1Test rig

Which can be schematized as:

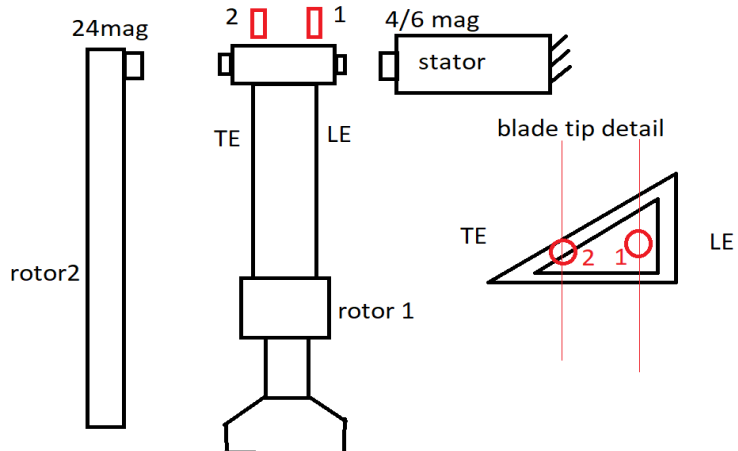


Figure 5.2 Test rig scheme

We can distinguish three main components:

- The Test Article (TA): which consists of a bladed disk with 144 blades
- A Rotating Magnet Carrier (MC): which has 24 magnets uniformly distributed along the circumference
- A static Magnet Carrier: which can have a total number of magnets equal to both 4 or 6 magnets

The experiment has been conducted in vacuum, meaning that the forcing does not have an aerodynamical source. That is why magnets have been adopted. In particular, the two different MCs allow to obtain two different kinds of excitation:

- *Asynchronous vibrations*: due to the rotating MC and the TA rotating in the same direction at different speeds. In detail, the TA rotates at a fixed speed for the whole experiment while the rotating MC undergoes a former phase of Acceleration and then decelerates. The frequency of the excitation is given by the gap in speed of the two rotors, meaning that when the MC is slow, the excitation has a high frequency. This frequency tends to decrease progressively as the MC accelerates. In the range of frequencies obtained there must a matching with the natural frequencies of the bladed disk. In particular, we are interested in the first two modes. When the matching occurs, then the blade resonates, and we have found a crossing on Campbell diagram.

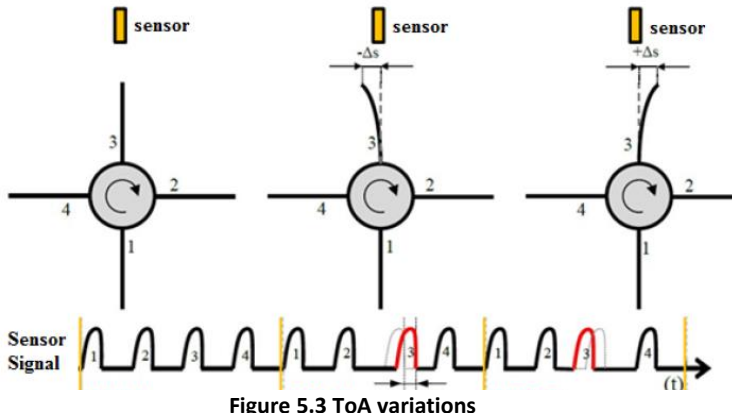
Adopting a MC with 24 magnets, also allows to investigate high EO, which is useful when modeling bladed disk's behavior to flutter.

- *Synchronous vibrations*: due to the static MC. In this case the TA is accelerated and then decelerated since the MC is fixed. The principle of how the crossing with natural frequencies on the Campbell diagram occurs is pretty much the same as the aforementioned for Asynchronous vibrations. In this case, we are also able to study low EO.
- *Overlap crossing type*: in this case the forcing comes both from the rotating and the static MCs.

According to what has been said so far, it is clear how frequency is known throughout all the experiment. Indeed, we were able to monitor the speed of both TA and rotating MC. Yet, In order to comprehensively extract useful information from the test, it is necessary to know also the amplitude. For this spinning test, an innovative method of acquiring the displacement of the blade tip has been used: the Blade Tip Timing (BTT) system.

5.1.1 Blade Tip Timing system

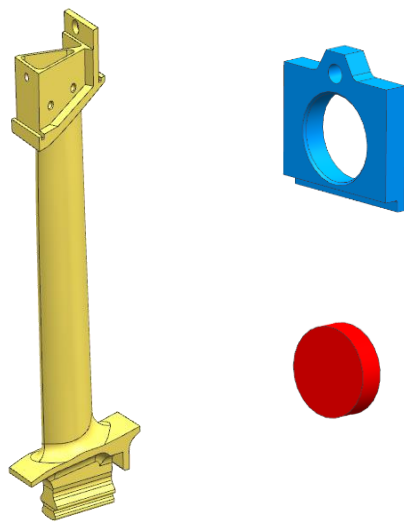
This system is based on a very simple concept; indeed, by using optical laser sensors it is possible to compare the predicted position of the blade at a precise Time of Arrival (ToA) to its actual position. The distance between the two points, corresponds to the displacement on the blade tip due to vibrations.



This method of measuring is preferred to the older one that uses strain gauges. That is due to the fact that the latter is an intrusive method; therefore, it can interfere with the modal behavior of the system itself.

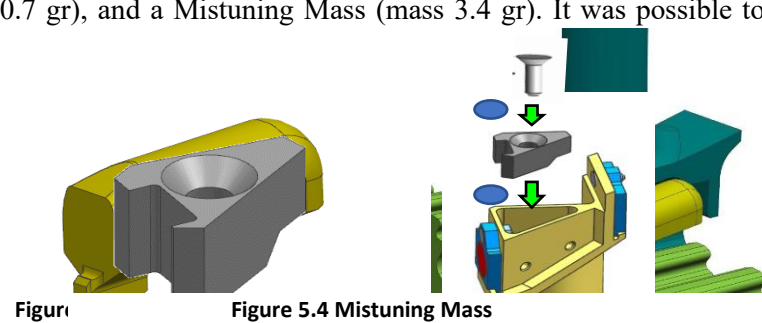
5.2 Test Article Design

As mentioned before, the TA for the Stargate spinning test consists of a bladed disk with 144 blades. Yet, since the main goal of this work is to be able to appreciate how intentional mistuning affects modal behavior of the system, several configurations have been tested. Starting from the Tuned configuration, which is taken as a baseline, an overview of the main components is provided.



As we can see from the picture, the single sector of the Tuned blade consists of a cantilever blade which is mechanically connected to a disk through four contact surfaces. On the tip of the blade, there have been installed two magnets (*Double Magnets Configuration*). The presence of two different magnets both on the Leading Edge (LE) and the Trailing Edge (TE) is due to the forcing coming from the MCs on each side respectively.

Two different elements have been adopted to introduce mistuning starting from the Tuned configuration: an Underplatform Damper, which can be made either of Steel (mass: 2.1 gr) or Aluminum (mass: 0.7 gr), and a Mistuning Mass (mass 3.4 gr). It was possible to obtain a set of



Figure

Figure 5.4 Mistuning Mass

different configurations by installing these elements on some specific blades in such a way to recreate a mistuning pattern. The mistuning mass was installed in an hollow made in the tip shroud, while the underplatform damper was installed in the interblade space between two adjacent blades.

More in detail, the configurations obtained are:

- Tuned
- Mistuned Mass 01
- Mistuned Mass 0001
- Tuned + Damper Aluminum
- Tuned + Damper Steel
- Mistuned Damper Aluminum 001
- Mistuned Damper Steel 001
- Mistuned Mass 01 + Damper Aluminum
- Mistuned Mass 01 + Damper Steel
- Mistuned Mass 0001 + Damper Aluminum
- Mistuned Mass 0001 + Damper Steel

Where 1 and 0 refer:

- For the mistuning mass: respectively to the blades that have been modified by adding the mistuning mass compared to the Tuned configuration blades or not. So, for example, Mistuned Mass 0001 is a configuration where the sector consists of four blades and the mistuning mass has been installed every fourth blade;
- For the underplatform damper: to the interblade space in which the damper has been installed. So, for example, Mistuned Damper Steel 001 is a configuration where the sector has three blades and the damper has been installed in every third interblade. In this case, the blades that are to be considered mistuned are the two that are in contact with the damper since this connection may affect modal behavior of those blades.

About the test article, it is also important to highlight other parameters that contributes to the variety of the tests. Indeed, it was possible to change not only the gap between the TA and each one of Magnet Carrier but also the magnet size. In this way, we were able to modulate the forcing. Varying all these parameters (Configuration, Corssing Type, TA Speed, Rotating/ Static Magnet Gap and Size), it was possible to test every possible combination.

6. DATA FITTING METHODS

6.1 Data format

In order to extract important modal parameters from acquired measurements, it was necessary to somehow sort out effectively the data. Indeed, the single test consists of a great number of measurements, which include not only the two different crossing with the first two modes for both acceleration and deceleration phases, but also all those points that are far from the peak response and are not useful for our purpose.

As we can see in the picture below, which represents the raw data related to a single test and a single mode. In this case, both acceleration and deceleration phases are plotted. By looking at the Frequency vs. Amplitude plot, we can notice how only one peak is noticeable; this is due to the fact that the natural frequency is pretty much the same for both phases, meaning that in the first plot, the two peaks are overlapped. Yet, by plotting the raw data as a function of Time (plot on the right), then we can notice two distinguished peaks both for acceleration and deceleration phases, as we expected. Another important thing to underline is that data were already pre-processed. Indeed, it is unlikely for the blade to have an exact zero response far from the peak. What have been done, was to discard points far from the crossing or that do not match fit criteria.

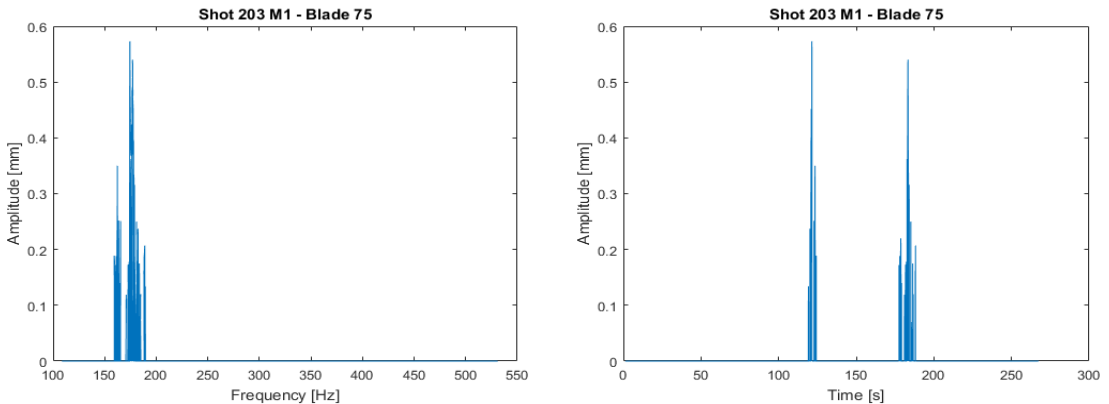


Figure 6.1 Frequency vs. Amplitude and Time vs. Amplitude plots o a generic test

The first step to start sorting out the data was to divide the two phases. To do so, we had to find the instant where the Magnet Carrier speed changes its trend; indeed, as the magnet carrier accelerates, the difference in speed between the MC and TA decreases. Therefore, the acceleration phase ends when the frequency of the forcing reaches a global minimum. From this point on we are interested in picking a limited number of points around the peak. Since the peak corresponds to the maximum

amplitude point, the next step is to fix a time range around the peak and discard all the points further from it. In this case, it was adopted a time range equal to 6 seconds, meaning that measurements outside the range $[t_{peak} - 3s; t_{peak} + 3s]$ are neglected.

In order to effectively fit the data and evaluate q-factor, all the points with zero amplitude among the remaining have been neglected as well. Moreover, not all the blades were considered when evaluating statistically significant values; indeed, an effort has been done neglecting all those blades which were affected with excessive noise or an erroneous data acquisition. This means excluding blades with unrealistically high peak amplitudes (Amplitudes higher than 7 mm) and blades affected by Non Synchronous Vibrations (NSV), in which the vibration source could not be reconnected to the MC. Finally, the last check on left points was to have at least 15 points in order to be able to track a significant Frequency Response Function (FRF) for the blade. A general end-of-pipe outcome is a data distribution like the one shown below.

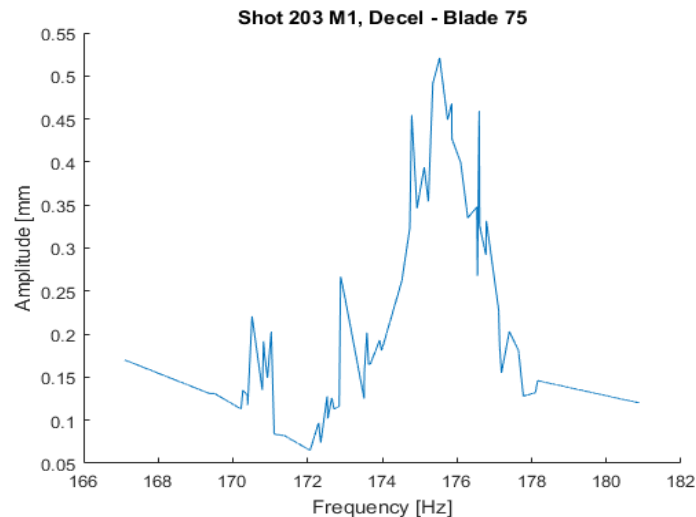


Figure 6.2 Data distribution after filtering

6.2 Methods used

Since there is not a simple analytical function that describes the experimental data as they are, the main goal of this part is to find a fitting curve that best interpolates points in the sense of least squares. By doing so, it will be easier to extract q-factor from the data distribution. When trying to find the best method, there are some relevant aspects to keep in mind:

- Whether the interpolating curve passes through the Peak of the FRF in terms of Frequency and Amplitude;

- Keeping the quadratic residue as little as possible, which can be expressed as:

$$qr = \sum_i (x - x_i)^2 \quad (6.1)$$

- Whether the interpolating curve can fit also points far from the peak.

6.2.1 Gauss-2 parameters

The first method used to interpolate data was the Gaussian curve, which is analytically defined as:

$$A = a \cdot e^{-\frac{(f-\omega_0)^2}{b}} \quad (6.2)$$

Where:

- a,b: parameters
- ω_0 : natural frequency

This kind of curve is centered in the frequency peak; yet the maximum of the curve is equal to the parameter a . Therefore, even though the curve will have its maximum at exactly the natural frequency, it is not said that it will also cross the peak in terms of amplitude.

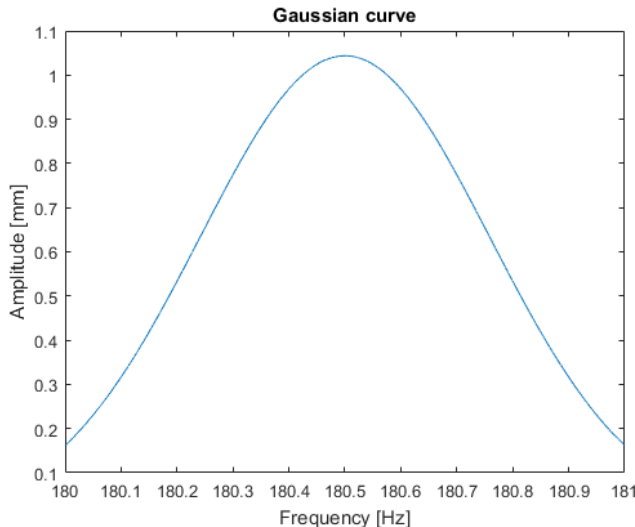


Figure 6.3 Gaussian curve

6.2.2 Gauss-1 parameter

In order to solve the problem of having the maximum at exactly the amplitude peak, another method that has been adopted is using a Gaussian curve similar to the one already shown. In this case, the parameter a is substituted by the peak amplitude:

$$A = A_{Peak} \cdot e^{-\frac{(f-\omega_0)^2}{b}} \quad (6.3)$$

By doing so, we are sure to match both peak frequency and amplitude. On the other hand, using less parameters in the interpolating curve, exposes us to committing a higher error for the other points (on the peak the error is null).

6.2.3 Kumaraswamy Distribution

The third method studied is the Kumaraswamy distribution. This kind of distribution is analytically described by:

$$A = cab \cdot f^{a-1} \cdot (1 - f^a)^{b-1} \quad (6.4)$$

Where a, b, c are parameters

The concept behind the choice of such function is to have as many parameters to operate on as possible in order to minimize quadratic residue. Unlikely, by leaving all these parameters optimizing the error, we cannot make any prevision about whether the curve will match peak amplitude or frequency.

6.2.4 Single Degree of Freedom Method

The last method studied is the one considering a *Single Degree of Freedom* (SDOF) system, which consists of a Mass-Spring-Damper structure like the one in the picture.

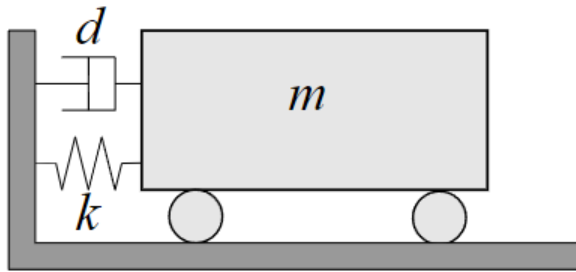


Figure 6.4 Mass-Spring-Damper system

The amplitude function of frequency of such system under an harmonic forcing is:

$$A = \frac{2\zeta A_{peak}}{\sqrt{\left(\frac{2f\zeta}{\omega_0}\right)^2 + \left(1 - \left(\frac{f}{\omega_0}\right)^2\right)^2}} \quad (6.5)$$

Where:

- ζ : damping parameter
- ω_0 : natural frequency

Differently from the Kumaraswamy distribution, the SDOF Method has as only one parameter the damping ζ . As we can see from the analytical formula, the fitting curve matches both peak amplitude and frequency, like the Gaussian-1 Parameter.

6.3 Methods comparison

The approach used to choose the best fitting method to apply on experimental data is to try to fit more simple functions. By using these simple analytical functions, we are able to calculate the exact value for damping by using:

$$Q_{factor} = \frac{f_0}{\Delta f} \quad (6.6)$$

Where:

- f_0 : natural frequency
- Δf : frequency range between the two so-called *half power points*. It is the difference between abscissas of the points that have an amplitude equal to the maximum amplitude divided by $\sqrt{2}$.

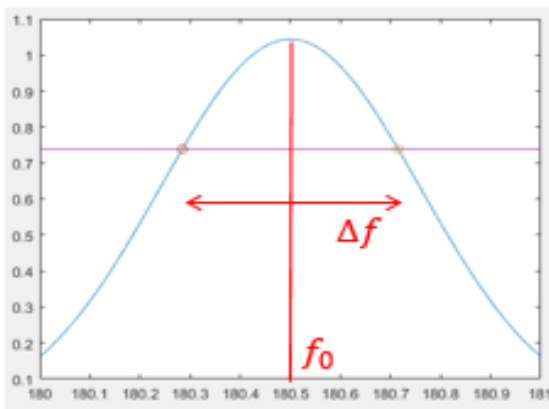


Figure 6.5 Parameters for Q-factor calculation

The simple functions that have been chosen to test the behavior of the four methods, were picked in such a way to represent some sort of peak in order to resemble as much as possible an average data distribution. Functions case of studies are:

- Triangular

$$A(f) = \begin{cases} 2 \cdot (f - 180), & 180 \leq f < 180.5 \\ 1 - 2 \cdot (f - 180), & 180.5 \leq f < 181 \end{cases}$$

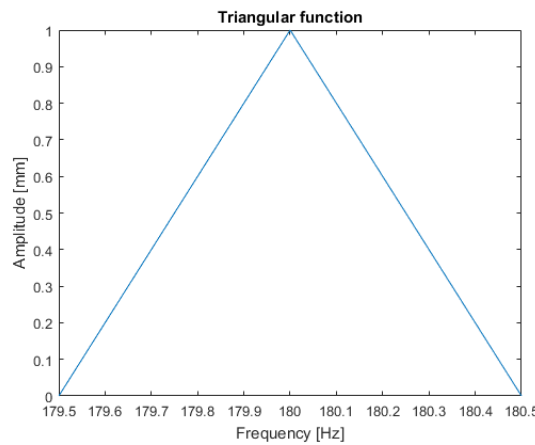


Figure 6.6 Triangular function

- Sinusoidal:

$$A = \sin\left(f + \frac{\pi}{2} - 180\right) \quad 180 - \frac{\pi}{2} < f < 180 + \frac{\pi}{2}$$

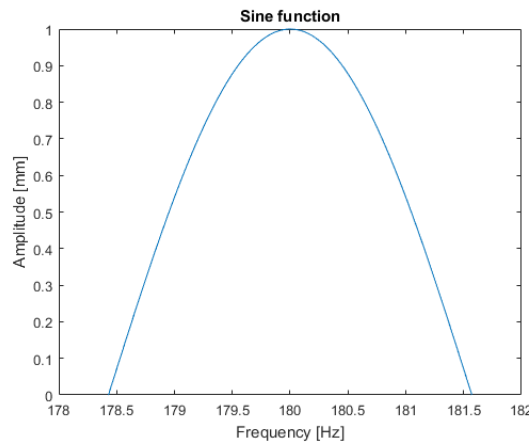


Figure 6.7 Sinusoidal function

- Parabolic:

$$A = -4 \cdot (f - 179.5)^2 + 4 \cdot (f - 179.5) \quad 179.5 < f < 180.5$$

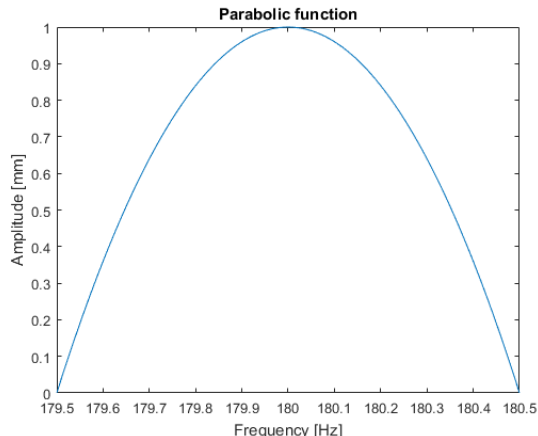
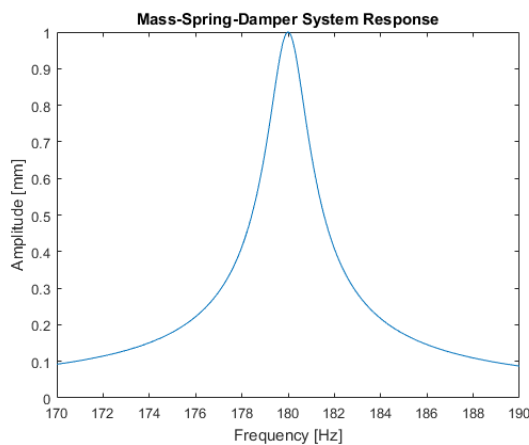


Figure 6.8 Parabolic function

- Mass-Spring-Damper System harmonic forced response:

$$A = \frac{f_0/k}{\sqrt{\left(1 - \left(\frac{f}{\omega_n}\right)^2\right)^2 + \left(\frac{2\zeta f}{\omega_n}\right)^2}} \quad \begin{cases} f_0 = 1 \\ k = 100 \\ \zeta = 0.005 \\ \omega_n = 180 \\ 170 < f < 190 \end{cases}$$

Where:



- f_0 : forcing modulus
- k : stiffness
- ζ : damping
- ω_n : natural frequency/peak frequency

Applying the interpolation methods that have been already shown to these functions:

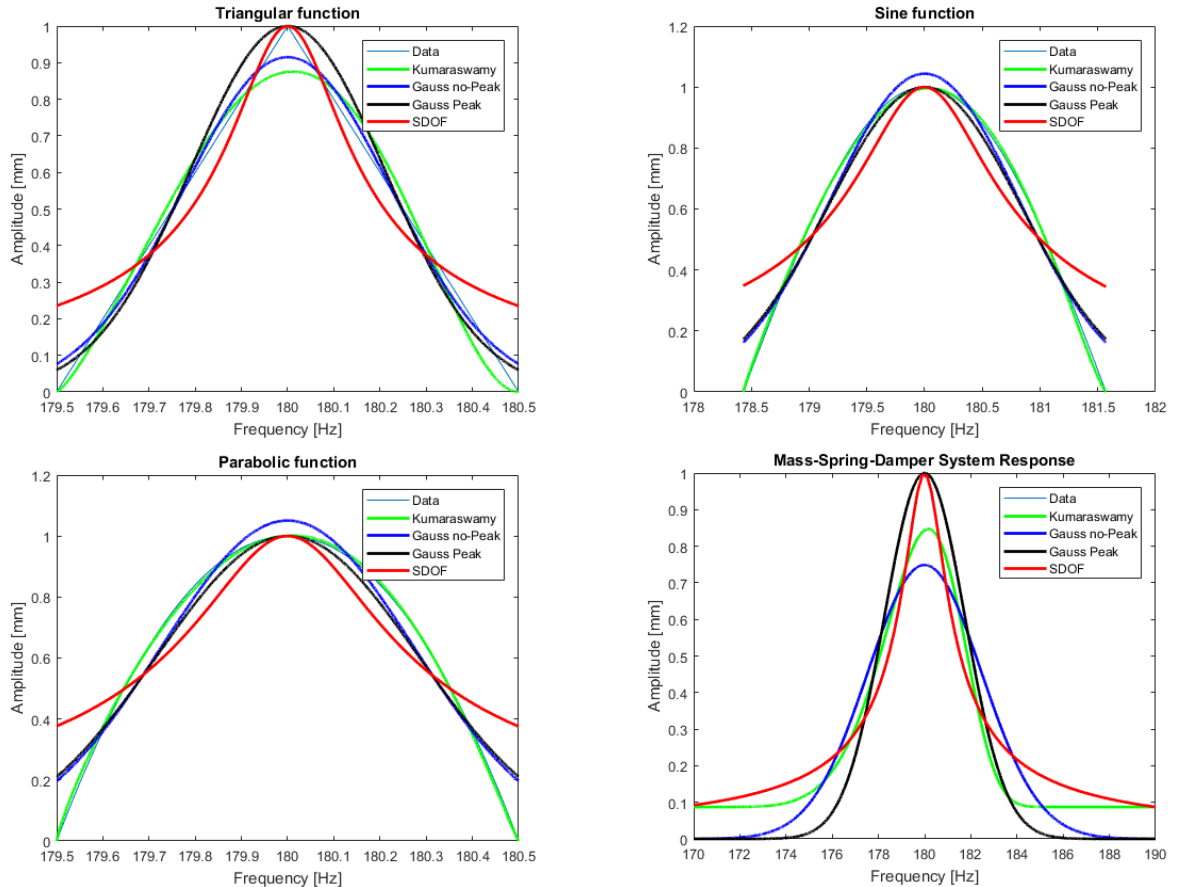


Figure 6.9 Methods applied to analytical functions

We are now able to compare the different methods. Looking at the results table below, we can see how in most cases having more parameters to vary minimizes the residue. Yet, a small error does not necessarily imply a more precise value when calculating q-factor. Even though, given the results, we would tend to choose the Kumaraswamy distribution as the best interpolation method; we eventually chose the SDOF Method. That is because, the SDOF method not only matches peak frequency and amplitude, but also seems to better approximate FRF tails further from the peak. Yet, this method has to be used with caution, since it works well on neat data distribution that do not present much noise or irregularity. In those cases, Kumaraswamy distribution method is still a valid alternative. As a matter of fact, the extraction of relevant statistical values has been done on the best experimental data, which means the ones having a clear peak and low scattering.

	Triangular		Parabolic		Sine		Mass-Spring-Damper	
	Q-factor	Quad. Residue	Q-factor	Quad. Residue	Q-factor	Quad. Residue	Q-factor	Quad. Residue
Analytic	614.6	-	332.6	-	114.6	-	100	-
Gauss no-Peak	481.9	0.306	396	0.637	132.9	0.5437	43.8	2.308
Gauss Peak	513.2	0.526	381.7	0.698	128.9	0.595	61.9	2.801
Kumaraswamy	422.9	0.453	334.3	0.1007	133.2	0.116	58.9	1.416
SDOF	743.5	0.91	443.4	1.354	155	1.341	100	1.50E-04

Table 1 Methods Comparison

To justify what has been said so far, we can see how the four methods behave when being applied on actual data:

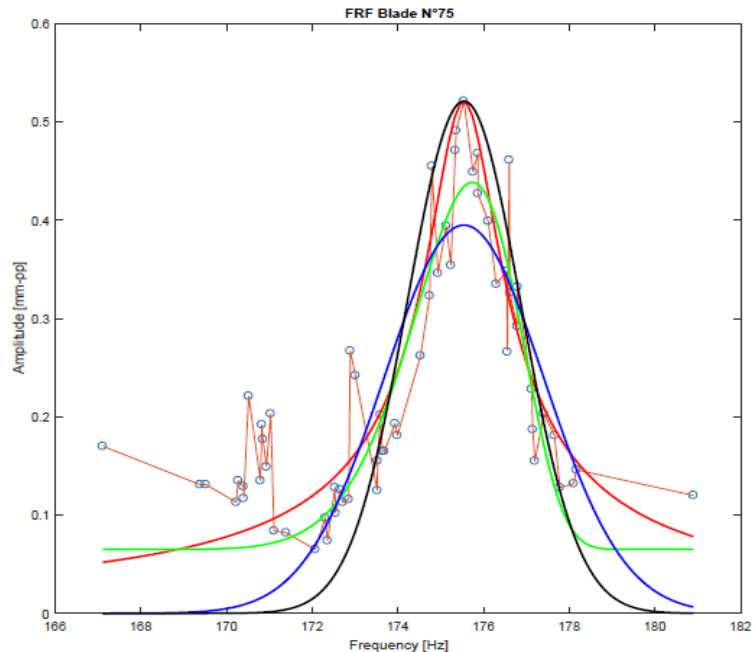


Figure 6.10 Shot 203 M1, Accel - Blade 75

	Gauss no-Peak	Gauss Peak	Kumaraswamy	SDOF
Q-factor	56.5	79.6	75.7	106.5
Quad. Residue	0.691	0.786	0.485	0.472

Table 2 Q-factor and Quadratic Residue using different methods

7. MATCHING WITH FEA

This section will focus mainly on the comparison in terms of natural frequency between the results obtained from the experimental data and the ones expected from a modal analysis on the corresponding FEM Model.

7.1 Modal analysis

In order to be able to compare natural frequencies, a modal analysis as shown in chapter 2 was necessary. Yet, in this case we wanted to study the behavior of a given configuration when changing the TA Speed and the EO. It is important to remember that a modal analysis is performed on the structure itself, without taking into account external forcing. That is why we are interested in comparing only the frequency, we would not have any information about the amplitude anyway. As said before, the angular velocity of a system, affects the modal behavior of the structure; therefore, we could not simply perform a single analysis on the system. Indeed, for every comparison we firstly selected the TA Speed at which the crossing with the natural frequency happened; then we performed a static analysis aiming at modelling the preload stress given by the centrifugal forces. Once performed the static analysis, we finally can proceed with the modal one. What we expect is that the natural frequencies increase with the angular velocity since the preload is higher and the structure is stiffer.

Particular attention has been paid to the contact surfaces between the disk sector and the blades. The contact type chosen in this zone is the *bonded* one. Differently from other architectures, there are not contacts at the blade interlocking. Moreover, either the damper, the mistuning mass and the magnets have been modelled as punctiform masses.

7.2 Tuned Configuration

Each one of the next sections is dedicated to the study of a single configuration. The first one is the Tuned Configuration, which has been taken as a baseline.

Shot	Crossing Type	Mode	TA Speed	Avg Amplitude	Std_dev Amplitude	Avg Frequency	Std_dev Frequency	Avg Qfactor	Std_dev Qfactor	Frequency FEA	Error in Frequency (%)
203	Asynch	M1	2000	0.416	0.101	174.5	3.3	67.4	24.9	171.3	1.86
203	Asynch	M2	2000	0.404	0.096	322.6	6	143.6	52.2	355.8	9.33
432	Asynch	M1	2500	0.511	0.129	182.6	2.5	85.1	32.1	178.7	2.18
432	Asynch	M2	2500	0.740	0.197	319.4	9.7	170.2	70.5	361.6	11.67
195	Synch	M1	1717	0.160	0.050	171.7	2.6	143.1	74.7	166.4	3.19
314	Synch	M1	2787	0.203	0.085	185.8	2.3	145.1	73.7	183.00	1.53

Table 3 Tuned Configuration results

FEA Results:

- TA Speed: 2000 RPM
- EO: 24

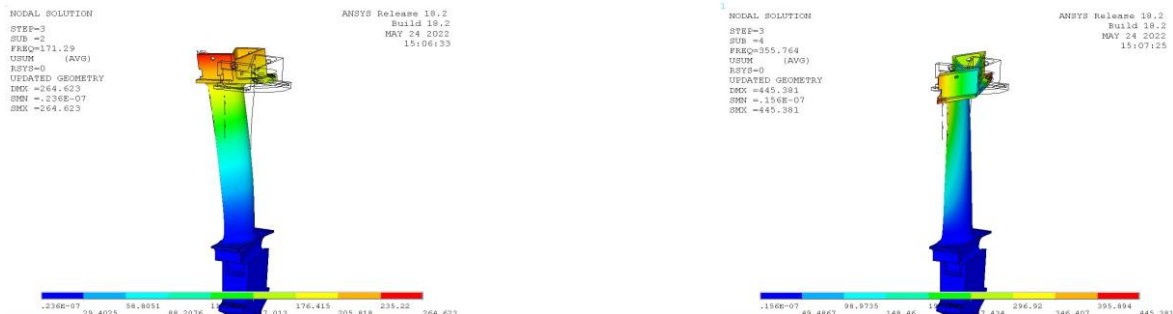


Figure 7.1 Tuned Configuration – Modeshapes for Mode 1 and 2

- TA Speed: 2500 RPM
- EO: 24

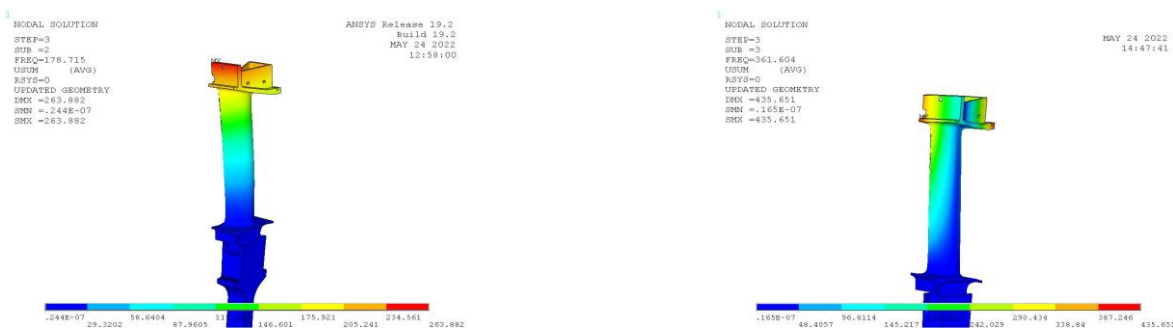


Figure 7.2 Tuned Configuration – Modeshapes for Mode 1 and 2

Error was calculated as:

$$Err = \frac{|F_{FEM} - F_{exp}|}{F_{FEM}} \quad (7.1)$$

For the Tuned Configuration, there seems to be a good matching in frequencies. In general, Mode 1 is less affected by error than Mode 2; indeed, as we will see for other configurations, the FEM Model tends to get stiffer than the actual TA making natural frequencies higher almost all the time.

7.3 Mistuned Mass 01 Configuration

In this configuration, mistuning has been introduced by using a mistuning mass on alternate blades. All those blades that have the mistuning mass installed will be called *blade 1*, otherwise *blade 0*. Differently from the Tuned Configuration, in this case it is necessary to study separately tuned and mistuned blades. The first step should hence be to identify mistuned blades and then evaluate statistical values for amplitude, frequency, and q-factor aside. Yet, since we already know that one every two blades present mistuning, it is sufficient to separate even and odd blades.

Shot	Crossing Type	Mode	TA Speed	Blade	Avg Amplitude	Std_dev Amplitude	Avg Frequency	Std_dev Frequency	Avg Qfactor	Std_dev Qfactor	Frequency from FEA	Error in Frequency (%)
419	Asynch	M1	2000	1	0.436	0.126	166.0	2.1	91.0	30.2	181.0	8.29
419	Asynch	M1	2000	0	0.408	0.095	173.9	3.5	92.5	26.4	193.2	9.99
419	Asynch	M2	2000	1	0.407	0.121	309.3	7.0	197.4	62.5	361.4	14.42
419	Asynch	M2	2000	0	0.416	0.096	322.0	6.2	170.8	53.0	388.4	17.10
175	Synch	M1	2363	1	0.300	0.094	175.7	2.3	111.8	61.2	189.4	7.23
175	Synch	M1	2790	0	0.210	0.065	186.0	3.5	91.3	63.5	202.5	8.15
415	Synch	M2	3190	1	0.218	0.166	319.0	7.5	209.5	105.7	365.1	12.63
415	Synch	M2	3261	0	0.325	0.187	326.1	5.0	240.4	92.9	392.0	16.81

Table 4 Mistuned Mass 01 results

FEA Results:

- TA Speed: 2000 RPM
- EO: 24
- Mode 1



Figure 7.3 Mistuned Mass 01 - Modeshape for Mode 1 blades 0 and 1

- TA Speed: 2000 RPM
- EO: 24
- Mode 2



Figure 7.4 Mistuned Mass 01 - Modeshape for Mode 2 blades 0 and 1

As said before, in this case the sector for cyclic symmetry consists of the two blades 0 and 1. Since the presence of the mistuning mass changes modal behavior of the blade, we can notice that the two modeshape, for the same mode, have different natural frequency. This can be already considered as an achievement since we managed to decouple blades behavior avoiding that the structure will ever resonates entirely. We can also notice how the error is bigger compared to Tuned Configuration, especially for Mode 2.

Another interesting thing to investigate is how energy is transmitted from a blade to another. Indeed, since all the blades are mechanically connected to the same disk, it may happen that when a blade

resonates at its natural frequency, we expect that part of the vibrational energy is transmitted to adjacent blades. In other words, even if we are far from the natural frequency of the blade itself, we would expect some response due to the excitement of adjacent blades.

By looking at the FRFs of two adjacent blades, we can see how the Mistuning Mass effectively changes natural frequencies of a blade; yet the energy transfer is small. Indeed, we cannot distinguish any clear secondary peak.

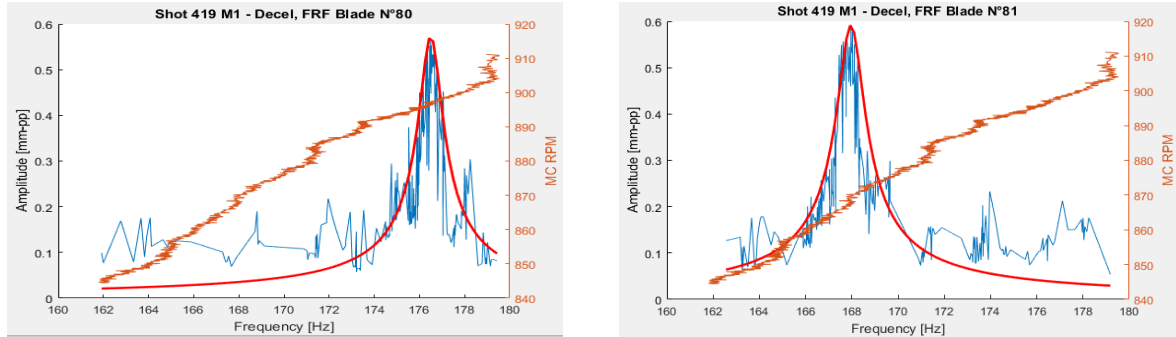


Figure 7.5 Mistuned Mass 01 - Adjacent blades FRFs

7.4 Mistuning Mass 0001

Similarly to the Mistuned mass 01 configuration, in this case the mistuning mass has been installed every fourth blade. In this case it was harder to identify blades 1. What we did was to firstly plot all the frequency per blade and then look for a pattern reoccurring every four blades. In particular we would expect. In particular, we were looking for lower peaks representing the frequency of those blades with the mistuned mass installed.

Shot	Crossing Type	Mode	TA Speed	Blade	Avg Amplitude	Std_dev Amplitude	Avg Frequency	Std_dev Frequency	Avg Qfactor	Std_dev Qfactor	Frequency from FEA	Error in Frequency (%)
Shot 141	Asynch	M1	1715	1	0.339	0.080	164.9	7.3	80.7	26.5	178.1	7.4
Shot 141	Asynch	M1	1715	0	0.427	0.112	171.1	3.2	99.4	25.6	190.3	10.1
Shot 153	Asynch	M2	2500	1	0.712	0.241	313.8	8.3	150.6	71.0	364.1	13.8
Shot 153	Asynch	M2	2500	0	0.834	0.439	324.7	6.6	176.1	75.9	390.2	16.8

Table 5 Mistuned Mass 0001 results

FEA Results:

- TA Speed: 1715 RPM
- EO: 24

- Mode 1



Figure 7.6 Mistuned Mass 0001 - Modeshape for Mode 1 blades 0 and 1

- TA Speed: 2500 RPM
- EO: 24
- Mode 2



Figure 7.7 Mistuned Mass 0001 - Modeshape for Mode 2 blades 0 and 1

Again, we can see how the blade 1 has different natural frequencies from the three blades 0. We can also notice how the error committed when comparing the FEA results to the experimental data is larger than previous configuration.

7.5 Tuned + Damper Steel

Even though it has been said that underplatform dampers can be used as an element to introduce mistuning, in this configuration they have been installed in every interblade space. This means that there will be no distinction between blade 0 and 1. Contrarily to the adoption of mistuning mass, we do not expect a large shift in natural frequencies using dampers. We would rather study its effect on amplitude.

Shot	Crossing Type	Mode	TA Speed	Avg Amplitude	Std_dev Amplitude	Avg Frequency	Std_dev Frequency	Avg Qfactor	Std_dev Qfactor	Frequency from FEA	Error in Frequency (%)
Shot 354	Asynch	M1	2000	0.415	0.214	174.5	4.3	87.8	33.4	192.9	9.54
Shot 354	Asynch	M2	2000	0.648	1.078	323.8	6.3	149.8	69.3	388.5	16.65
Shot 355	Asynch	M1	2500	0.718	0.287	185.8	5.3	73.9	23.2	200.6	7.38
Shot 355	Asynch	M2	2500	0.552	0.149	322.5	7.0	246.3	74.9	390.3	21.02
Shot 368	Synch	M1	2835	0.164	0.075	189.0	2.8	219.3	90.9	205.1	7.85
Shot 349	Synch	M2	3289	0.299	0.114	328.9	5.0	291.9	96.3	391.3	16.10

Table 6 Tuned + Damper Steel results

FEA Results:

- TA Speed: 2000 RPM
- EO: 24



Figure 7.8 Tuned + Damper Steel Configuration – Modeshapes for Mode 1 and 2

- TA Speed:
- EO: 24



Figure 7.9 Tuned + Damper Steel Configuration – Modeshapes for Mode 1 and 2

We can also study whether the presence of an underplatform damper between two blades affects the way in which vibrational energy is transmitted from a blade to the adjacent one, like it has been done for Mistuned Mass 01 configuration. Looking at the picture below, we can notice how the two peak frequencies are very similar; this is concordant to the fact that the blade itself is not modified by the damping, so we do not expect large shifts in frequency. Yet, we can see clearly secondary peaks in

both of the FRFs due to the excitation of the adjacent blade. We can conclude that dampers effectively transfer vibrational energy.

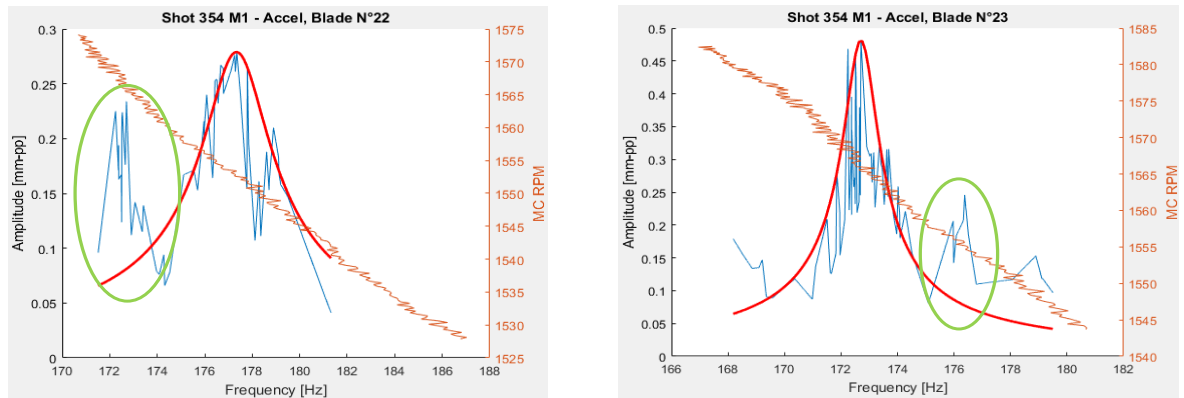


Figure 7.10 Tuned + Damper Steel - Adjacent blades FRFs

7.6 Tuned + Damper Aluminum

Shot	Crossing Type	Mode	TA Speed	Avg Frequency	Std_dev Frequency	Frequency from FEA	Error in Frequency (%)
Shot 251	Asynch	M1	2500	188.5	6.7	190.9	5.97
Shot 251	Asynch	M2	2500	323.0	6.3	388.1	17.11

Table 7 Tuned + Damper Alu results

This is the last configuration among the ones studied. The sector scheme is the same as the Tuned + Damper Steel, that is because we are interested in how the choice of the material for the underplatform damper affects peak amplitude.

FEA Results:

- TA Speed: 1715 RPM
- EO: 24

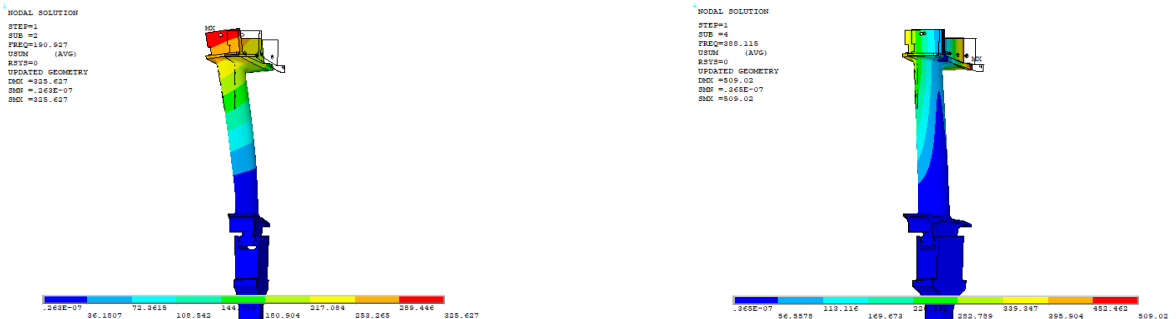


Figure 7.11 Tuned + Damper Alu Configuration – Modeshapes for Mode 1 and 2

- TA Speed: 2500 RPM
- EO: 24



Figure 7.12 Tuned + Damper Alu Configuration – Modeshapes for Mode 1 and 2

As we can see, the percentage error committed when comparing frequency is higher. This is due to uncertainties on the average natural frequency in experimental data. Indeed, looking at the peak frequency per blade plot below, the distribution of peaks is not around a single value but around two. This makes the prediction of the true natural frequency even harder since the average value loses its statistical significance.

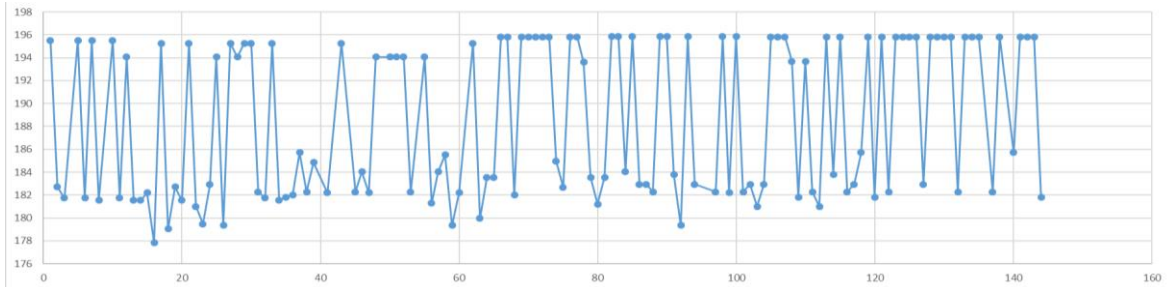


Figure 7.13 Frequency per blade

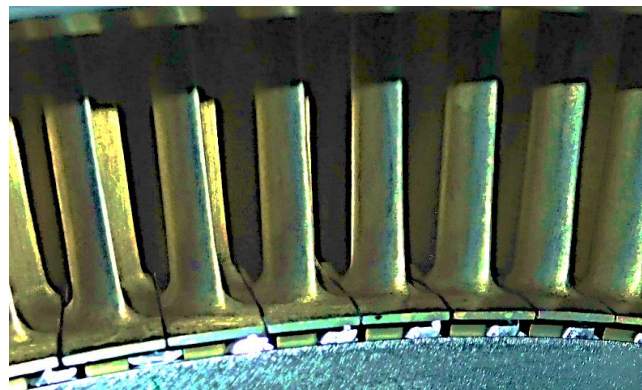


Figure 7.14 TA and Dampers closeup

This behavior may be reconducted to how the dampers have been installed. As we can notice by the picture, the dampers are play-mounted meaning that during the experiment they could lightly move relatively to the structure affecting its behavior. Moreover, the figure below shows a comparison of

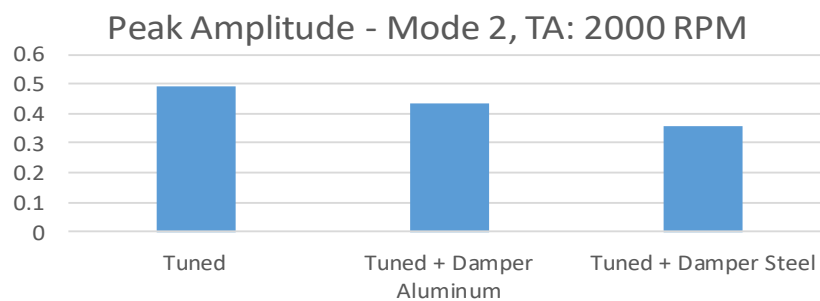


Figure 7.15 Underplatform Damper effect on average Peak Amplitude

the average peak amplitude between either the Tuned, Tuned + Damper Steel and Tuned + Damper Alu configurations. As we can see, the presence of dampers effectively affects oscillations amplitude. More in detail, steel dampers seem to better influence damping; this may be due to the higher stiffness of the damper itself.

8. CONCLUSIONS

We have seen how the Single Degree of Freedom Method seems the best to interpolate experimental data. Yet, when data distribution is affected by noise or the peak is not so neat, it is also convenient to adopt a method that minimizes quadratic residue by using more parameters for the interpolation, like the Kumaraswamy distribution.

The results agree with what we expected since the mistuning masses effectively affect natural frequencies of the blade and dampers were able to reduce oscillation amplitude. This is a positive achievement since we either managed to decouple blades behavior and not to let the entire structure resonate at the same frequency, avoiding disastrous failures.

The post-processed data will be useful for further research in aeromechanics for a better understanding of flutter and forced response using mistuning. For this purpose, all the results have been shared with all the partners of ARIAS project.

BIBLIOGRAPHY

- [1] Kenneth W. Bushell. "Jet and Gas Turbine Engines", in Encyclopedia of Physical Science and Technology (Third Edition), 2003
- [2] Aviation-history.com/engines/turbojet.htm
- [3] Aviation-history.com/engines/turbofan.htm
- [4] Aviation-history.com/engines/turboprop.htm
- [5] S.L. Dixon B. Eng., Ph.D., C.A. Hall Ph.D. "Axial Flow Turbine", in Fluid Mechanics and Thermodynamics of Turbomachinery (Sixth Edition), 2010
- [6] Denis Laxalde, Jean-Pierre Lombard, Fabrice Thouverez. "Dynamics of Multistage Bladed Disks Systems", in Journal od Engineering for gas Turbines and Power, American Society of Mechanical Engineers, 2007, 129 (4), pp.1058-1064. 10.1115/1.2747641
- [7] Jacquet-Richardet, G., Ferraris, G., Rieutord,P. "Frequencies and modes of rotating flexible bladed disk-shaft assemblies: a global cyclic symmetry approach", in Journal of Sound and Vibration, Volume 191, Issue 5, 18 April 1996, pages 901-915
- [8] Paul Petrie-Repar, Proposal Submission Form: Advanced Research Into Aeromechanical Solutions, 2017
- [9] Alberto Civardi: MS thesis - Development and validation of algorithms for vibration monitoring of aeronautical engines, 2020
- [10] Artur J. Lemonte, "Improved point estimation for the Kumaraswamy distribution", In: Journal of Statistical Computation and Simulation vol. 81, 2011 issue 12
- [11] Brayton cycle. url: https://en.wikipedia.org/wiki/Brayton_cycle
- [12] Pierre C. «Mode Localization and Eigenvalue Loci Veering Phenomena in Disordered Structures». In: Journal of Sound and Vibration 126 (1988), pp. 485–502
- [13] Mehrdad Pourkiaee, Stefano Zucca, Robert G. Parker. "Relative cyclic component mode synthesis and its application to nonlinear vibration of mistuned bladed disks with friction joints
- [14] Dewey H. Hodges and G. Alvin Pierce. Introduction to structural dynamics and aeroelasticity. Vol. 15. Cambridge University Press, 2011
- [15] A.V. Srinivasan. «Flutter and resonant vibration characteristics of engine blades», in Journal of Engineering for Gas Turbines and Power 119 (4), October 1997, pages 742-775
- [16] Wake. url: <https://en.wikipedia.org/wiki/Wake>
- [17] Tom O'Haver. "A pragmatic Introduction to Signal Processing"
- [18] M. Rades. "Comparison of vibration properties", in Encyclopedia of Vibration (20001), pages 272-277.
- [19] https://en.wikipedia.org/wiki/Normal_distribution

